Pattern formation in Stochastic Partial Differential Equations

Harry Saxton
Project Supervisor: Dr. Mariya Ptashnyk

Declaration

I, Harry Saxton, confirm that this work submitted for assesment is my own and is expressed in my words. Any uses made within it of the works of other authors in any form e.g. ideas, equations, figures, text, tables, programs, are properly acknowledged at any point of their use. A list of references employed is included.

Signature: H.Saxton

Acknowledgement

Abstract

This thesis is a computational and analytical look of reaction diffusion systems, which are coupled PDEs describing the diffusion behaviour and reaction of two interacting chemicals. Under certain conditions, such systems are able to generate stationary patterns of finite characteristic wave lengths. The properties of the resulting patterns are determined internally by the diffusion and reaction rates of the chemicals. In research Turing patterns have been shown to have an important place in the world and thus reaction diffusion systems which exhibit Turing patterns could provide a credible way to model the processes involved in biological problems. Turing patterns are born out of certain models due to diffusion-driven instability which is caused by infinitesimal perturbations around a spatially homogeneous steady state of a model. Systems have been studied using mathematical tools and numerical simulations. We then consider noise as an input to the system which gives us a pair of coupled SPDEs. Using numerical simulations we will be able to investigate the behaviour and the impact that noise plays on generating these Turing patterns.

Contents

Chapter 1

Introduction

In nature patterns can be observed in various different parts of it, these extend from patterning of the human veins to complex sand dunes even in embryonic development. These mechanisms, such as diffusion driven instability, which cause patterning are involved heavily in both the animal and plant kingdoms. What mechanisms regulate pattern formation and how animals get the patterns on their coats is still a relevant question in todays research [1, 2, 3]. Until recently we had very little knowledge on how organisms that exist in this world develop into much larger complex organisms, even with new research for the most part we don't understand most of the biological systems in our world. One of the main reasons for this is the large amount of diversity that exists in the animal and plant kingdom. During the initial stages of embryonic development mechanisms occur which create the organism, however the mechanisms involved in creating the spatial patterns on the organism i.e it's organs, body parts etc are still widely unknown. Despite there been many different proposed theories over the years, very little progress has been made in the field of developmental biology. Before the beginning of the 20th century there were only descriptive theories, none of which could be verified experimentally. In the 1960s new ideas arose which also came alongside new computers, using these scientists were able to shed a bit more light on the mechanisms involved. Now it seemed as if we could study naturally occurring phenomena experimentally. Pattern formation has been proposed as one of the main explanations as to how the homogenous division of cells can lead to spatial pattern formation in embryos [4, 5]. Some may argue that genes play an important role in the formation of patterns, genes do answer a lot of questions regarding the mechanisms that are involved in the developmental stage. However, on their own they are not sufficient enough to provide an explanation for the spatial distribution of patterns.
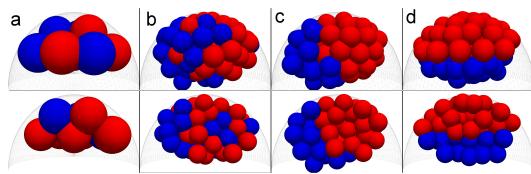

Figure 1.1: A 3D simulation of the early stages on embryonic development [6]

1

It is obvious that other processes must undergo the steps required for pattern formation. In a survey made among developmental biologists [7],a large proportion referred to the molecular processes of morphogenesis and how patterns are established in the early embryonic development as one of the most interesting and difficult problems that is unsolved in biological sciences today.

Models used to describe the formation of patterns in the past have been a mixture of both stochastic and deterministic ones. Models which are subject to no noise are termed deterministic, ones that undergo some noise are termed stochastic. One way to think about noise is that noise in a model can account for random effects that we can't possibly accurately model. As an examples some types of noise are white noise, Brownian noise, Gaussian noise and Levey noise please refer to [8, 9, 10] for an indepth discussion on the different types of noise. Noise is a ever-present occurrence in the natural world and will always play a vital role in impacting biological systems. Hausenblas et al. [33] investigated stochastic Gray-Scott equations proving some existence results for the equations while also simulating the deterministic and stochastic equations and showing how the patterns can vary when the noise is a independent spatially time-homogeneous Wiener processes. Surulescu and Kelkel [34] investigated the stochastic Gierer–Meinhard system they prove the existence of a positive solution for the resulting system then use numerical simulations to characterize pattern formation on seashells under the influence of random space–time fluctuations. Sun et al. [11] showed that noise can make a circle pattern transform into target wave-like patterns thorugh numerical simulations. Scarsoglio et al. [12] presented different stochastic processes of spatial pattern formation using a variable as a noise effect in the system. Hori and Hara [13] provided a mechanistic basis of Turing pattern formation through inducing internal noise. Many studies have been presented in these research areas [14, 15, 16], however theory on Turing bifurcation and pattern formation in biological systems was rarely studied.

This thesis will begin with formulating the general models of reaction-diffusion systems and stochastic reaction diffusion systems we shall analyse the systems through a range of stability analysis and numeric in order to look for Turing type pattern formation. The idea that diffusion can destabilise the specially homogeneous steady sate of a model and result in formation of periodic patterns was first investigated by Alan Turing. This was revolutionary, since usually diffusion have smoothing and stabilising effect. However a specific relation between diffusion coefficients in the system and reaction we obtain diffusion driven instability and those reaction-diffusion systems can model patterns observed in nature. He published the mathematical theory in his seminal paper "The Chemical Basis of Morphogenesis" [17] in 1952. Similar analysis will be performed on the deterministic systems, then considering a specific type of perturbation we will derive conditions for when we can expect Turing patterns to appear when a specific type forcing is present in a system. Then we shall investigate the effect of stochastic forcing on our reaction diffusion systems .

The aim of this thesis is to investigate and analyse the effect of noise and sensitivity

of biological systems. We then round off the thesis by examining a model of chemotaxis and exploring the effect of noise, seeing how this affects the behaviour of the deterministic model.

Chapter 2

Reaction Diffusion and Chemotaxis Equations

Here we shall consider the general set up for all of the equations that we shall analyse in this thesis.

2.1 Deterministic Reaction Diffusion (DRD)

The general deterministic reaction diffusion system has the form

$$\frac{\partial u}{\partial t} = D_u \Delta u + f(u, v), \text{ in } D \times (0, T),$$
$$\frac{\partial v}{\partial t} = D_v \Delta v + g(u, v) \text{ in } D \times (0, T),$$

$$(2.1)$$

$$D_u \nabla u \cdot \nu = 0 \text{ and } D_v \nabla v \cdot \nu = 0 \text{ on } \partial D \times (0, T),$$
$$u(0) = u_0, \ v(0) = v_0 \text{ on } D.$$

$$(2.2)$$

Where $D \subset \mathbb{R}^d$ is a bounded, Lipschitz domain.

We assume that we have two chemicals $u(\mathbf{x}, t), v(\mathbf{x}, t)$ that will react and diffuse. Here $f(u, v), g(u, v)$ control the reaction kinetics of the two chemicals. $D_u, D_v > 0$ are the diffusion coefficients, and $u_0, v_0 > 0$ are the inital conditions for the system. We shall assume that we also have a positive spatially homogeneous steady state (u_s, vs), satisfying $f(u_s, v_s) = g(u_s, v_s) = 0$.

Notice that the non-linearities in (2.1) depend on the variables u, v and not on the partial derivatives of u and v. Such equations are called semilinear problems.

We will now define each of the individual models that we shall study here.

2.1.1 FitzHugh–Nagumo model (FHN)

The FitzHugh–Nagumo model (FHN), is named after Richard FitzHugh who first created the system in 1961, then J. Nagumo et al. extended the model to describe an excitable system e.g a neuron. FitzHugh–Nagumo model [18, 19] is a relaxation oscillator because, if the stimulus which is created externally exceeds a certain threshold value, the system will show a limit cycle in its phase space, then the variables u and v will clam and relax back to their inital pre stimulus levels. This behaviour is often seen in spike generations which is a short, nonlinear increase in the voltage of the membrane u, which is diminished over time by a slower, recovery variable v, which is linear. The equations that describe this system take the form

$$
\begin{aligned}
\frac{\partial u}{\partial t} &= (a - u)(u - 1)u - v + D_u \Delta u, \\
\frac{\partial v}{\partial t} &= e(bu - v) + D_v \Delta v,
\end{aligned}
\tag{2.3}
$$

together with the initial and boundary conditions (2.2). The $a, e, b > 0$ are the reaction rates for each individual reaction.

2.1.2 Brusselator model (Bru)

The Brusselator model is a theoretical realisation for an autocatalytic reaction. The Brusselator model was proposed by Ilya Prigogine and his coworkers [20].

The non-dimensional model reads

$$
\begin{aligned}
\frac{\partial u}{\partial t} &= a - (b + 1)u + v^2 y + D_u \Delta u, \\
\frac{\partial v}{\partial t} &= bu - u^2 v + D_v \Delta v,
\end{aligned}
\tag{2.4}
$$

together with the initial and boundary conditions (2.2). Here $a, b > 0$ are constants of the reaction.

2.1.3 Schnakenberg model (Sch)

In 1979 Schnakenberg [21] described a system that demonstrates oscillations in a simple chemical network. The non-dimensional model reads

$$
\begin{aligned}
\frac{\partial u}{\partial t} &= a - u + u^2 v + D_u \Delta u, \\
\frac{\partial v}{\partial t} &= b - u^2 v + D_v \Delta v,
\end{aligned}
\tag{2.5}
$$

together with the initial and boundary conditions (2.2). Here $a, b > 0$ are constants of the reaction.

2.2 Peturbed Reaction Diffusion (PRD)

We now make a slight extension to our general reaction diffusion system (2.1) by incorporating a deterministic perturbation around the steady state. This perturbation around the steady state will ensure that the solutions remain positive, due to our assumption of a positive steady state. The general equations are

$$
\begin{aligned}
\frac{\partial u}{\partial t} &= D_u \Delta u + D_1 R_1(u,v)\zeta_1 + f(u,v), \\
\frac{\partial v}{\partial t} &= D_v \Delta v + D_2 R_2(u,v)\zeta_2 + g(u,v),
\end{aligned}
\tag{2.6}
$$

We use the same boundary and initial conditions specified in (2.2). We define the perturbation terms to be

$$
\begin{aligned}
\zeta_1 &= \frac{1}{\sqrt{2\pi}\sigma} e^{-\frac{(u-u_s)^2}{2\sigma^2}}, \\
\zeta_2 &= \frac{1}{\sqrt{2\pi}\sigma} e^{-\frac{(v-v_s)^2}{2\sigma^2}},
\end{aligned}
\tag{2.7}
$$

and

$$
\begin{aligned}
R_1(u,v) &= u - u_s, \\
R_2(u,v) &= v - v_s.
\end{aligned}
\tag{2.8}
$$

So we can see the noise terms follow the distributions similar to a normal distribution. It is important to remember this is not a random variable just a deterministic perturbation. This choice of perturbation will aide us when we derive the analytical conditions for pattern formation which will become apparent later.

2.2.1 Perturbed FitzHugh–Nagumo model (PFHN)

The perturbed system (2.3) is given by

$$
\begin{aligned}
\frac{\partial u}{\partial t} &= (a-u)(u-1)u - v + D_u \Delta u + D_1(u-u_s)\zeta_1, \\
\frac{\partial v}{\partial t} &= e(bu-v) + D_v \Delta v + D_2(v-v_s)\zeta_2,
\end{aligned}
\tag{2.9}
$$

where ζ_1, ζ_2 are defined in (2.7). We also implore the same boundary and initial conditions stated in (2.2). $D_1, D_2 > 0$ are our perturbation magnitudes.

2.2.2 Perturbed Brusselator Model (PBru)

Considering the perturbation in system (2.4) the model reads

$$
\begin{aligned}
\frac{\partial u}{\partial t} &= a - (b+1)u + u^2 v + D_u \Delta u + D_1(u-u_s)\zeta_1, \\
\frac{\partial v}{\partial t} &= bu - u^2 v + D_v \Delta v + D_2(v-v_s)\zeta_2,
\end{aligned}
\tag{2.10}
$$

6

where ζ_1, ζ_2 are defined in (2.7). We also implore the same boundary and initial conditions stated in (2.2). $D_1, D_2 > 0$ are perturbation magnitudes.

2.2.3 Perturbed Schnakenberg Model (PSch)

Adding the perturbation to the system (2.5) the model reads

$$
\begin{aligned}
\frac{\partial u}{\partial t} &= a - u + u^2 v + D_u \Delta u + D_1(u - u_s)\zeta_1, \\
\frac{\partial v}{\partial t} &= b - u^2 v + D_v \Delta v + D_2(v - v_s)\zeta_2,
\end{aligned}
\tag{2.11}
$$

where ζ_1, ζ_2 are defined in (2.7). We also implore the same initial and boundary conditions stated in (2.2). $D_1, D_2 > 0$ are our perturbation magnitude.

2.3 Stochastic Reaction Diffusion (SRD)

We now consider an extension of the basic deterministic reaction diffusion system in order to accommodate for space-time noise. The general equations read

$$
\begin{aligned}
du(t,x) &= [D_1 \Delta u + f(u,v)]dt + \sigma_1(u,v)dW(t) \text{ in } D \times (0,T), \\
dv(t,x) &= [D_2 \Delta v + g(u,v)]dt + \sigma_2(u,v)dW(t) \text{ in } D \times (0,T),
\end{aligned}
\tag{2.12}
$$

where $W(t)$ is the Q-Wiener process. A good way to think of this term is as the derivative of a Q-Wiener process see definition (2.6). We then also will refer to $\sigma_1(u,v), \sigma_2(u,v)$ as our noise intensity. We also use the same boundary and initial conditions specified in (2.2). In the stochastic setting we can either have additive or multiplicative noise. If the noise is additive this is the situation where $\sigma_1(u,v)$ and $\sigma_2(u,v)$ are constant. If the noise is multiplicative noise this means that the noise pertubation depends on the variable itself. Which is the situation in which we shall consider our numerical simulations in chapter 4. Now we have the general set up for SRD equations we shall provide a definition for what a Q-Wiener process actually is.

We first give the definition of a filtered probability space

Definition 2.4. Let $(\Omega, \mathcal{F}, P)$ be a filtered probability space which consists of our sample space Ω, a set of events $\mathcal{F}$ and a probability measure P.

- A filtration $\{\mathcal{F}_t : t \geq 0\}$ is a family of sub σ-algebras of $\mathcal{F}$ that are increasing. $\mathcal{F}_s$ is a sub σ-algebra of $\mathcal{F}_t$ for $s \leq t$. Each $(\Omega, \mathcal{F}_t, P)$ is a measure space and we assume it is complete.

- A filtered probability space is a quadruple $(\Omega, \mathcal{F}, \mathcal{F}_t, P)$ where $(\Omega, \mathcal{F}, P)$ is a probability space and $\{\mathcal{F}_t : t \geq 0\}$ is a filtration of $\mathcal{F}$.

Stochastic processes that conform to the notion of time described by the filtration above are known as adapted processes

Definition 2.5 (Adapted). Let $(\Omega, \mathcal{F}, \mathcal{F}_t, P)$ be a filtered probability space. We say a Stochastic process $X(t)$ is $\mathcal{F}_t$-adapted if the random variable $X(t)$ is $\mathcal{F}_t$ measurable for all time.

We now define the standard Wiener process over this filtered probability space.

Definition 2.6 (Wiener Process). We say $\{W(t) : t \in \mathbb{R}^+\}$ is a Wiener process if it is a real valued Gaussian process with continuous sample paths, with a mean function $\mu(t) = E[W(t)] = 0$ and covariance function C(t,s)=min{t,s}. Also we can say that W(t) is a Weiner process such that

1. W(0)=0.

2. The increments $W(t) - W(s) \sim N(0, t - s)$ for $t \geq s$ and the increments over disjoint intervals are independent of $\mathcal{F}$ for $s < t$.

3. W(t) is continuous as a function of t for each $\omega \in \Omega$.

This is then often the forcing that is used to study SDEs however we notice that it has no spatial dependence at all. We first need a couple of definitions from [**30**] in order to define a Q-Weiner process

Definition 2.7 (uncorrelated, covariance operator). A linear operator $\eta : L^2(D) \implies L^2(D)$ is the covariance of $L^2(D)-$valued random variables X and Y if

$$\langle \eta\theta, \psi \rangle = Cov(\langle X, \theta \rangle, \langle Y, \psi \rangle), \forall \theta, \psi \in L^2(D),$$

where $Cov(X, Y) = E[(X - E[X])(Y - E[Y])^T]$ and we can define

$$\langle X, Y \rangle_{L^2(\Omega, L^2(D))} = \int_\Omega \langle X(\omega), Y(\omega) \rangle dP(\omega) = E[\langle X, Y \rangle].$$

In the case that X=Y we say that η is the covariance of X

From the above the definition we then can derive the following lemma

Lemma 2.7.1. Let $X \in L^2(D)$ with mean μ and covariance operator η. The covariance operator η is symmetric non-negative definite and is of trace class with Tr= $E[||X - \mu||^2]$

We are now in a position to properly define our Q-Wiener process, define the Q-Wiener process $\{W(t) : t \geq 0\}$ as a $L^2(D)$-valued process. Each W(t) is a $L^2(D)$-valued Gaussian random variable and each has a well defined covariance operator. The covariance operator at t=1 is denoted Q and by lemma 2.7.1, it must satisfy the following assumption

Assumption 2.7.2. $Q \in L^2(D)$ is non-negative definite and symmetric. Also Q has an orthonormal basis $\{\gamma_j : j \in \mathbb{N}\}$ of eigenfunctions with corresponding eigenvalues $q_j \geq 0$ such that $\sum_{j \in \mathbb{N}} q_j < \infty$ i.e Q is of trace class.

Recalling the Definition 2.4,2.5 above we can define the Q-Wiener process

Definition 2.8 (Q-Wiener Process). A $L^2(D)$-valued stochastic process $\{W(t) : t \geq 0\}$ is a Q-Wiener process if

1. $W(0) = 0$,

2. $W(t)$ is a continuous function $\mathbb{R}^+ \implies L^2(D)$ for each $\omega \in \Omega$,

3. $W(t)$ is $\mathcal{F}_t$-adapted and $W(t) - W(s)$ is independent of $\mathcal{F}$ for $s < t$ and,

4. $W(t) - W(s) \sim N(0, (t-s)Q)$ for all $0 \leq s \leq t$,

where Q satisfies assumption 2.72.

We can also represent the Q-Wiener process as a linear combination of the eigenfunctions γ_j of Q.

Theorem 2.8.1. Let Q satisfy Assumption 2.7.2. Then W(t) is a Q-Wiener process if and only if

$$W(t) = \sum_{j=1}^{\infty} \sqrt{q_j} \gamma_j \beta_j(t),$$

where $\beta_j(t)$ are identically independently distributed $\mathcal{F}_t$-Wiener processes and the series converges in $L^2(\Omega, L^2(D))$. γ_j are the eigenfunctions of Q and q_j are the eigenvalues of Q.

For the proof see [**30**] p.g 437.

We will now define all our specific stochastic models which we shall use to reference back to later.

2.8.1 Stochastic FitzHugh–Nagumo model (SFHN)

Using the non-dimensional equations (2.3) we add the extra noise term we then have the SFHN,

$$\begin{aligned} du &= [(a-u)(u-1)u - v + D_u \Delta u]dt + \sigma_1(u,v)dW(t), \\ dv &= [e(bu-v) + D_v \Delta v]dt + \sigma_2(u,v)dW(t). \end{aligned} \tag{2.13}$$

We also implore the same boundary and initial conditions used in (2.2).

2.8.2 Stochastic Brusselator Model (SBru)

Adding the additional noise term to the system (2.4) we get

$$
\begin{aligned}
du &= [a - (b+1)u + u^2v + D_u\Delta u]dt + \sigma_1(u,v)dW(t), \\
dv &= [bu - u^2v + D_v\Delta v]dt + \sigma_2(u,v)dW(t),
\end{aligned}
\tag{2.14}
$$

we also implore the same boundary and initial conditions used in (2.2)

2.8.3 Stochastic Schnakenberg Model (SSch)

Finally, adding the noise term to system (2.5) the model reads

$$
\begin{aligned}
du &= [a - u + u^2v + D_u\Delta u]dt + \sigma_1(u,v)dW(t), \\
dv &= [b - u^2v + D_v\Delta v]dt + \sigma_2(u,v)dW(t),
\end{aligned}
\tag{2.15}
$$

we implore the same initial and boundary conditions used in (2.2).

2.9 Chemotaxis

Chemotaxis occurs when a cell is stimulated to move as a result of a chemical attractant. For example skeletal formation during embryonic development cells often display directed movement as a result of chemicals [**26**, **27**], an example of this is cell aggregation as a result of cAMP waves, which we will talk about more in detail soon.

We will set up a general system where the cell density u travels up the gradient of a chemical v. If a cell moves up a chemical gradient (i.e. towards high concentrations of the chemical) then the chemical is known as a chemoattractant, conversely if a cell moves down a chemical gradient (i.e. towards low concentrations of the chemical) then the chemical is known as a chemorepellent.

2.9.1 Chemotaxis System (DCS)

Given a cell density u and a chemical concentration v we can set up the general system of equations for chemotaxis.

$$
\begin{aligned}
\frac{\partial u}{\partial t} &= D_u\Delta u - \chi\nabla(u\nabla v) + f(u) \ \text{ in } D \times (0,T), \\
\frac{\partial v}{\partial t} &= D_v\Delta v + g(u,v) \ \text{ in } D \times (0,T).
\end{aligned}
\tag{2.16}
$$

Here we see we have used the same homogeneous Neumann boundary and initial conditions as in (2.2).

Where $\chi\nabla(u\nabla v)$: is the chemotactic term with u moving towards high concentrations of v. χ is commonly referred to as the chemotactic sensitivity. $f(u)$ this is responsible for cell kinetics, We specify that the cell kinetics depend only on the cell density u – this is because the chemical does not effect cell proliferation, only cell motility. This only works when considering pattern formation many models of chemotaxis cell proliferation is controlled by the chemical e.g. wound healing, immune response. $g(u,v)$ is the chemoattractant kinetics that depend on both u and v.

We also assume that we have a positive spatially homogenous steady state (u_s, v_s) such that $f(u_s) = g(u_s, v_s) = 0$.

2.9.2   Perturbed Chemotaxis System

We now add a deterministic forcing.

$$\begin{aligned}
\frac{\partial u}{\partial t} &= D_u\Delta u - \chi\nabla(u\nabla v) + f(u) + D_1 R_1(u)\zeta_1 \ \text{ in } D \times (0, T), \\
\frac{\partial v}{\partial t} &= D_v\Delta v + g(u, v) + D_2 R_2(u, v)\zeta_2 \ \text{ in } D \times (0, T),
\end{aligned} \tag{2.17}$$

please refer to (2.7) and (2.8) for descriptions of the forcing terms in the new equation, we also use the same initial and boundary conditions as in (2.2).

2.9.3   Stochastic Chemotaxis System

We now add a stochastic counterpart (2.12).

$$\begin{aligned}
du &= [D_u\Delta u - \chi\nabla(u\nabla v) + f(u)]dt + \sigma_1(u, v)dW(t) \ \text{ in } D \times (0, T), \\
dv &= [D_v\Delta v + g(u, v)]dt + \sigma_2(u, v)dW(t) \ \text{ in } D \times (0, T),
\end{aligned} \tag{2.18}$$

where σ_1, σ_2 are the intensity of the noise. The boundary and initial conditions are the same as those specified in (2.2)

We will now detail a specific model of chemotaxis that we shall analyse. Before we go into this we shall provide a biological background to motivate the problem

2.9.4   lifecycle of Dictyostelium discoideum (Dd)

Cellular slime molds, such as Dictyostelium discoideum (Dd), are soil based microorganisms with a fascinating life cycle. In their natural environment they play a crucial role in breaking down decaying material, however it is their ability to cooperate that has long fascinated scientists [28] .

In an abundant food supply Dd function as individual "amoeboid" cells, consuming the

available food, undergoing cellular division and the population expands. However, as the food becomes exhausted, the cells start to cooperate and accumulate to form an aggregation mound composed of approximately 100000 cells. Within this mound, cells differentiate into two principal cell types: stalk and spore cells. The mound evolves into a multicellular slug which migrates to a suitable location until assembling to form a fruiting body. The stalk cells sacrifice themselves by forming a long stalk and protective casing that contains the spore cells. The spore cells remain dormant until either the wind or an animal transplants them to a more favourable location [29].

The lifecycle of Dd has become an important model system for studying how cells are capable of communicating and behaving as a collective system. In this section we shall address by modelling the important first step of this process: namely, how the initially individual cells are capable of assembling to form the aggregation mound.

There are some biological facts that these cells have to abide by which will impact the creation of our model

1. As cells begin to starve, they start to produce and secrete a chemical called cAMP.

2. cAMP is a chemoattractant for the Dictyostelium cells.

3. cAMP is degraded by specific enzymes (called proteolytic enzymes).

Deterministic Dd

Considering $u(\mathbf{x}, t)$ the density of the Dictyostelium cells and $v(\mathbf{x}, t)$ as the concentration of the chemical chemoattractant (cAMP). We specify the kinetic terms stated which were not specified in the general model (2.16)

$$
\begin{aligned}
f(u) &= ru(1 - u), \\
g(u, v) &= au - bv.
\end{aligned}
\tag{2.19}
$$

$ru(1 - u)$ models the logistic growth of Dictyostelium cells, with a growth rate r, au describes the production of cAMP by Dictyostelium cells at a rate a, and bv models the degradation of cAMP by proteolytic enzymes at a rate b.

Note cAMP does not effect cell proliferation, only cell motility.

For all of these systems such as (2.1) and (2.12) full proofs of well posedness have been investigated in [37, 38, 39], see appendix C for the main Theorems. However moving forward it is assumed that all systems investigated have Existence and uniqueness, Existence for all times, Continuous dependency on the initial conditions and due to us dealing with biological systems we place two extra conditions on them Solution is non-negative for non-negative initial data and Solution is bounded for all bounded initial data.

Chapter 3

Turing and Hopf bifurcation

Pattern formation can be summarised by a Turing bifurcation, which causes the spatially homogeneous steady state to move from stable to unstable. However the system can go to a globally oscillating homogeneous state with a dominant wave number k = 0, this leads to patterns in time this is characterised by a Hopf Bifurcation. If both are satisfied we get patterns in both time and space. In this chapter we shall derive the conditions needed to induce such bifurcations in deterministic and perturbed reaction diffusion systems.

3.1   Deterministic setting

In order to establish under what conditions (2.1) can model pattern formation we need to determine the conditions for which the spatially homogeneous steady state is

1. stable to a spatially homogeneous perturbation,

2. unstable to an inhomogeneous perturbation.

These conditions are given the name "Diffusion-Driven Instability (DDI)" or a "Turing instability" after Alan Turing [17], the first person to propose this mechanism for pattern formation. The expression "Diffusion–Driven Instability" refers to the fact that it is the presence of the diffusion terms which allows patterns to develop – without these terms the spatially homogeneous steady state is stable.

To derive these conditions analytically first we linearise (2.1) around the spatially homogeneous steady state (u_s, v_s). We define

$$U(\mathbf{x}, t) = u(\mathbf{x}, t) - u_s,$$
$$V(\mathbf{x}, t) = v(\mathbf{x}, t) - v_s.$$

(3.1)

Subbing into the RDS (2.1) and retaining only the linear order terms we get the following linearised system.

$$\frac{\partial U}{\partial t} = D_u \Delta U + f_u U + f_v V,$$
$$\frac{\partial V}{\partial t} = D_v \Delta V + g_u U + g_v V,$$

(3.2)

where $f_u = \frac{\partial f}{\partial u}|_{(u_s,v_s)}, f_v = \frac{\partial f}{\partial v}|_{(u_s,v_s)}, g_u = \frac{\partial g}{\partial u}|_{(u_s,v_s)}, g_v = \frac{\partial g}{\partial v}|_{(u_s,v_s)}$, are the derivatives of the kinetic functions evaluated at the steady states.

We look for solutions of the form

$$U(\mathbf{x}, t) = \bar{U}(t)e^{ik\mathbf{x}},$$
$$V(\mathbf{x}, t) = \bar{V}(t)e^{ik\mathbf{x}},$$

(3.3)

Where $e^{ik\mathbf{x}} = cos(k\mathbf{x}) + isin(k\mathbf{x})$.

This implies that we expect any spatial patterns to develop to be periodic in space with wavelength $2\pi/k$. k is referred to as the wavenumber.
Subbing (3.3) into the linearised system (3.2) to obtain

$$\frac{d}{dt}\begin{bmatrix} \bar{U} \\ \bar{V} \end{bmatrix} = A\begin{bmatrix} \bar{U} \\ \bar{V} \end{bmatrix}, \quad \text{where } A = \begin{bmatrix} f_u - D_u k^2 & f_v \\ g_u & g_v - D_v k^2 \end{bmatrix}$$

(3.4)

We can see easily that

$$Tr(A) = (f_u + g_v) - (D_u + D_v)k^2,$$

(3.5)

$$Det(A) = \delta(k^2) = D_u D_v k^4 - (D_u g_v + D_v f_u)k^2 + f_u g_v - f_v g_u.$$

(3.6)

Finding the characteristic equation of our stability matrix A

$$\lambda^2 - Tr(A)\lambda + \delta(k^2) = 0.$$

From this we can identify the eigenvalues of our stability matrix as

$$\lambda = \frac{1}{2}(Tr(A) \pm \sqrt{Tr^2(A) - 4\delta(k^2)}.$$

(3.7)

Given 2 eigenvalues λ_1, λ_2 from stability analysis we know that a steady state is stable if

$$Re(\lambda_1), Re(\lambda_2) < 0,$$

looking at the form of our eigenvalues we can say that our steady state is stable if and only if

$$Tr(A) < 0 \ \& \ Det(A) > 0.$$

Conversely, we can say that a steady state is unstable if

$$Re(\lambda_1) > 0 \text{ or } Re(\lambda_2) > 0,$$

14

once again using the form of our eigenvalues we can say a steady state is unstable if and only if

$$Tr(A) > 0 \ or \ Det(A) < 0$$

Looking back at what conditions were required for our steady state we have that it is

1. Stable to a homogeneous perturbation $\iff$ Steady state is stable when $k = 0$ $\iff$ Tr(A) < 0 & Det(A)>0, when $k = 0$

2. Unstable to an inhomogeneous perturbation $\iff$ Steady state is unstable, when $k > 0$ $\iff$ Tr(A) > 0 or Det(A)<0, when $k > 0$

Hence, using the trace and determinant of the stability matrix A defined above, we can now start to see the first conditions needed for DDI.

1. Stable to a homogeneous perturbation requires

$$Tr(A) < 0 \ \text{for} \ k = 0 \iff f_u + g_v < 0 \quad \text{(DDI 1)}$$

and

$$Det(A) > 0 \ \text{for} \ k = 0 \iff f_u g_v - f_v g_u > 0 \quad \text{(DDI 2)}$$

.

2. Unstable to an inhomogeneous perturbation requires either $Tr(A) > 0$ or $Det(A) < 0$ for at least one positive value of k^2.

We know that $Tr(A) = (f_u + g_v) - (D_u + D_v)k^2$ however from DDI 1 this implies that $Tr(A) < 0, \ \forall k$. Hence instability can only occur when $Det A < 0$.

$Det(A) = \delta(k^2) = D_u D_v k^4 - (D_u g_v + D_v f_u)k^2 + f_u g_v - f_v g_u$ is a quadratic in k^2 with a minimum value δ_{min} when $k^2 = k_{min}^2$.

Solving $\delta(k^2)$ for its roots and taking the positive one we find that

$$k_{\min}^2 = \frac{D_u g_v + D_v f_u}{2 D_u D_v},$$

$$\delta_{\min} = (f_u g_v - f_v g_u) - \frac{(D_u g_v + D_v f_u)^2}{4 D_u D_v}.$$

Thus, we derive the final two conditions, $Det(A) < 0$ for some $k^2 > 0$ if and only if the following are satisfied

$$k_{min}^2 > 0 \iff D_u g_v + D_v f_u > 0 \quad (DDI3)$$

and

$$\delta_{min} < 0 \iff (D_u g_v + D_v f_u)^2 > 4 D_u D_v (f_u g_v - f_v g_u) \quad (DDI4)$$

So the 4 equations

$$
\begin{aligned}
Tr(A) < 0 \text{ for } k = 0 &\iff f_u + g_v < 0 \ (DDI1) \\
Det(A) > 0 \text{ for } k = 0 &\iff f_u g_v - f_v g_u > 0 \ (DDI2) \\
k_{min}^2 > 0 &\iff D_u g_v + D_v f_u > 0 \ (DDI3) \\
\delta_{min} < 0 \iff (D_u g_v + D_v f_u)^2 &> 4 D_u D_v (f_u g_v - f_v g_u) \ (DDI4)
\end{aligned}
\tag{3.8}
$$

complete our set of conditions for Diffusion-Driven Instability.

We shall also look for conditions for which a Hopf bifurcation may occur in a system. Although a Hopf bifurcation can occur at any wave number we consider the case where the leading wave number is $k = 0$. This will allow for simpler analysis. This then makes

$$
\begin{aligned}
Tr(A) &= (f_u + g_v), \\
Det(A) &= \delta(0) = (f_u g_v - f_v g_u).
\end{aligned}
\tag{3.9}
$$

Considering (2.1) we suppose that it has a spatially homogeneous fixed point e.g $(u, v) = (u_s, v_s)$. Let the eigenvalues of the linearised system (3.2) be given by $\lambda_{1,2} = \alpha(\mu) \pm i\beta(\mu)$. Suppose further that further for a certain value of μ the following conditions are satisfied:

1. $\beta(\mu_0) \neq 0$

2. $\alpha(\mu_0) = 0$

3. $\frac{d\alpha}{d\mu}(\mu_0) \neq 0$ i.e The transversality condition: the eigenvalues cross the imaginary axis with non-zero speed

The original paper can be found in [35] with the translation to english in [36]. Comparing these conditions to our eigenvalues (3.7,3.9) we can derive 3 conditions that must be staisfied in order for a Hopf bifurcation to occur

1. $\delta(0) = (f_u g_v - f_v g_u) > 0$

2. $Re(\lambda) = (f_u + g_v) = 0$

3. $\frac{d(Re(\lambda))}{d\mu}(\mu_0) \neq 0$ i.e transversality condition: the eigenvalues cross the imaginary axis with non-zero speed

Given μ as a bifurcation parameter of the system (2.1).

3.2   Perturbed Setting

In this section we now derive analytical conditions for which patterns can occur when our system is perturbed by a deterministic forcing. From system (2.6) the extra terms in the system are defined by (2.7) and (2.8). Here we are closely following the work of [29].

To examine the stability of the system and derive the new Turing conditions for pattern formation we consider a perturbation around the uniform steady state (u_s, v_s)

$$
\begin{aligned}
U(\mathbf{x}, t) &= u(\mathbf{x}, t) - u_s, \\
V(\mathbf{x}, t) &= v(\mathbf{x}, t) - v_s.
\end{aligned}
\tag{3.10}
$$

Plugging into our system (2.6) we then keep only linear order terms we derive the linearised system for our perturbed system

$$
\begin{aligned}
\frac{\partial U}{\partial t} &= D_u \Delta U + D_{11} U + f_u U + f_v V, \\
\frac{\partial V}{\partial t} &= D_u \Delta V + D_{21} V + g_u U + g_v V.
\end{aligned}
\tag{3.11}
$$

Compared to (3.2), we have two additional terms $D_{11}U, D_{21}V$.

We linearise around the steady state

$$
U(t) = u - u_s \implies u = U + u_s.
$$

Subbing into the noise term we get

$$
D_1(U + u_s - u_s)\frac{1}{\sqrt{2\pi}\sigma}e^{-\frac{(U+u_s-u_s)^2}{2\sigma^2}} = \frac{D_1}{\sqrt{2\pi}\sigma}Ue^{-\frac{U^2}{2\sigma^2}},
$$

Taylor expanding this to order $O(U^2)$ we get the additional forcing term

$$
\frac{D_1}{\sqrt{2\pi}\sigma}U.
$$

The same derivation applies for the noise term in the v equation.

Hence we define the following forcing terms that appear in the linearised system (3.11)

$$
\begin{aligned}
D_{11} &= \frac{D_1}{\sqrt{2\pi}\sigma}, \\
D_{21} &= \frac{D_2}{\sqrt{2\pi}\sigma}.
\end{aligned}
\tag{3.12}
$$

As in the deterministic setting we assume solutions to $P = \begin{bmatrix} U(t) \\ V(t) \end{bmatrix}$ have the form

$$
P = \begin{bmatrix} \bar{U}(t) \\ \bar{V}(t) \end{bmatrix} e^{ik\mathbf{x}},
$$

17

plugging the solutions into the system (3.11) we obtain the following

$$P_t = SP, \text{ Where } S = \begin{bmatrix} A_{11} - k^2 D_u & A_{12} \\ A_{21} & A_{22} - k^2 D_v \end{bmatrix} \tag{3.13}$$

where $A_{11} = f_u + D_{11}, A_{12} = f_v, A_{21} = g_u, A_{22} = g_v + D_{21}$.

We shall first derive the conditions for a Hopf bifurcation.

The characteristic equation from stability matrix S gives us the eigenvalues, which note have the same form as the deterministic setting (3.7),

$$\lambda = \frac{1}{2}(Tr(S) \pm \sqrt{Tr^2(S) - 4\delta(k^2)}, \tag{3.14}$$

where we have that, expanding the forms fully

$$Tr(S) = f_u + g_v + D_{11} + D_{21} - k^2(D_u + D_v), \tag{3.15}$$

$$\delta(k^2) = Det(S) = f_u g_v + f_u D_{21} + D_{11} g_v + D_{11} D_{21} - f_v g_u - (f_u D_v + D_{11} D_v + g_v D_u + D_u D_{21})k^2$$
$$+ D_u D_v k^4. \tag{3.16}$$

To derive the new Hopf conditions we based on bifurcation theory and what we derived in section one we see the following conditions have to be satisfied given an arbitrary bifurcation parameter $\mu = \mu_0$.

1. $\delta(0) = f_u g_v + f_u D_{21} + D_{11} g_v + D_{11} D_{21} - f_v g_u > 0$,

2. $Re(\lambda) = f_u + g_v + D_{11} + D_{21} = 0$,

3. $\frac{d(Re(\lambda))}{d\mu}(\mu_0) \neq 0$.

Comparing these conditions to the deterministic setting we see that condition 3 is identical as D_{11}, D_{21} are constants for a given σ. What we do see though is that condition 1 & 2 have the extra noise terms involved in them. It may be possible for us to achieve a Hopf bifurcation for a greater range of parameter values.

Now moving onto the new conditions required for a Turing bifurcation.

For point one we derive the first two conditions from our stability matrix S for k=0.

$$f_u + g_v + D_{11} + D_{21} < 0 \iff Tr(S) < 0 \quad (PDDI1)$$

and

$$f_u g_v + f_u D_{21} + D_{11} g_v + D_{11} D_{21} - f_v g_u > 0 \iff Det(S) > 0 \quad (PDDI2)$$

18

For point 2 we know $Tr(S) < 0 \; \forall k$ so we need Det(S)> 0 looking for a positive k_{min}^2 we solve $\delta(k^2)$ (3.17) we then find that

$$k_{\min}^2 = \frac{f_u D_v + D_{11} D_v + g_v D_u + D_{21} D_u}{2 D_u D_v},$$

and

$$\delta_{\min} = 4 D_u D_v (f_u g_v + f_u D_{21} + D_{11} g_v + D_{11} D_{21} - f_v g_u) - (f_u D_v + D_{11} D_v + g_v D_u + D_{21} D_u)^2.$$

Hence we arrive at our final two conditions

$$(f_u D_v + D_{11} D_v + g_v D_u + D_{21} D_u) > 0 \iff k_{\min}^2 > 0 \quad \text{(PDDI3)}$$

and

$$(f_u D_v + D_{11} D_v + g_v D_u + D_{21} D_u)^2 > 4 D_u D_v (f_u g_v + f_u D_{21} + D_{11} g_v + D_{11} D_{21} - f_v g_u)$$
$$\iff \delta_{\min} < 0 \quad \text{(PDDI4)}$$

So our complete set of equations then becomes

$$f_u + g_v + D_{11} + D_{21} < 0 \iff Tr(S) < 0 \quad \text{(PDDI1)}$$
$$f_u g_v + f_u D_{21} + D_{11} g_v + D_{11} D_{21} - f_v g_u > 0 \iff Det(S) > 0 \quad \text{(PDDI2)}$$
$$(f_u D_v + D_{11} D_v + g_v D_u + D_{21} D_u) > 0 \iff k_{\min}^2 > 0 \quad \text{(PDDI3)}$$
$$(f_u D_v + D_{11} D_v + g_v D_u + D_{21} D_u)^2 > 4 D_u D_v (f_u g_v + f_u D_{21} + D_{11} g_v + D_{11} D_{21} - f_v g_u)$$
$$\iff \delta_{\min} < 0 \quad \text{(PDDI4)}$$
$$(3.17)$$

PDDI 1-4 then make up the conditions needed to induce patterns for stochastic reaction diffusion systems. Once again I expect that these conditions will allow for a greater range of parameter values to be used in which these conditions will be satisfied and patterning will occur.

One important point to take from this chapter is that either one of the two bifurcations can occur at anyone one time this is due to the trace of our stability matrix always been less than zero for a Turing bifurcation where as when looking for a Hopf bifurcation we require the trace of our stability matrix to be equal to zero.

3.3 Examples of biological systems

3.3.1 FitzHugh-Nagumo model

In this section we shall use the conditions (3.8) and (3.17) to investigate the FHN and the PFHN to investigate what constraints need to be on the parameters in the model in order for patterns to appear.

Deterministic FHN

Recalling the system (2.3) we look for a spatially homogenous steady state we set

$$(a - u)(u - 1)u - v = 0, \ \ e(bu - v) = 0$$

solving we these equations we find our steady state to be

$$(u_s, v_s) = (\frac{1 + a + \sqrt{(1 - a)^2 - 4b}}{2}, bu_s).$$

Following the notation described in equation (3.2) we find that

$$f_u = 2a + 3b - (a + 1)\frac{1 + a + \sqrt{(1 - a)^2 - 4b}}{2}, \ \ f_v = -1, \ g_u = be, \ g_v = -e. \quad (3.18)$$

Then using the DDI conditions we derived (3.7) we can see what constraints will be placed on parameters in order for patterns to emerge

1. $f_u + g_v < 0 \implies (2a + 3b - (a + 1)\frac{1 + a + \sqrt{(1-a)^2 - 4b}}{2}) < e$

   Gives us a condition for the size needed on e.

2. $f_u g_v - f_v g_u > 0 \implies b > (2a + 3b - (a + 1)\frac{1 + a + \sqrt{(1-a)^2 - 4b}}{2}).$

   Using condition 1 we can gain the inequality $b > e$.

3. $D_v f_u + D_u g_v > 0 \implies \frac{D_v}{D_u} > \frac{e}{(2a + 3b - (a+1)\frac{1 + a + \sqrt{(1-a)^2 - 4b}}{2})}.$
   As we know e is a positive parameter we can conclude from this that f_u will also be positive in order to have a positive diffusion ratio.

4. $(D_u g_v + D_v f_u)^2 > 4 D_u D_v (f_u g_v - f_v g_u)$
   We can solve this to show that $d_c = \frac{D_v}{D_u}$ satisfys

$$d_c = \frac{2 f_u g_v - 4 f_v g_u + \sqrt{[2 f_u g_v - 4 f_v g_u]^2 - 4 f_u^2 g_v^2}}{2 f_u^2} \quad (3.19)$$

Plugging in the expressions for f_u, f_v, g_u, g_v

$$d_c = \frac{-2e(2a + 3b - (1 + a)\frac{1 + a + \sqrt{(1-a)^2 - 4b}}{2}) + 4eb + \sqrt{A}}{2(2a + 3b - (1 + a)\frac{1 + a + \sqrt{(1-a)^2 - 4b}}{2})^2}$$

Where $A = [-2e(2a + 3b - (1 + a)\frac{1 + a + \sqrt{(1-a)^2 - 4b}}{2}) + 4eb]^2 - 4(2a + 3b - (1 + a)\frac{1 + a + \sqrt{(1-a)^2 - 4b}}{2})^2 e^2$

Note solving condition 4 for D_v/D_u provides us with the critical diffusion bifurcation point d_c where when $D_v/D_u > d_c$ the steady state loses its stability and patterns can begin to form.

Following the general formulation from above we know the eigenvalues tale the form of (3.7). Here we are checking the conditions for a Hopf bifurcation hence the leading wave number here is k=0. So the trace and determinant have are (3.9) From the conditions we have derived for a Hopf bifurcation we have

1. $f_u g_v - f_v g_u > 0$ this condition holds if we assume the condition 2 for a Turing bifurcation hold

2. $f_u + g_v = 0 \implies e = (2a + 3b - (a+1)\frac{1+a+\sqrt{(1-a)^2-4b}}{2})$

3. $Re(\lambda)$ is not a constant, see the real part of the eigenvalue is

$$\alpha(e) = -e + 2a + 3b - (a+1)\frac{1+a+\sqrt{(1-a)^2-4b}}{2}$$

Hence, we see $\alpha'(e) = -1 \neq 0$.

Hence if all these conditions for a Hopf bifurcation hold we can say that at

$$e = 2a + 3b - (a+1)\frac{1+a+\sqrt{(1-a)^2-4b}}{2},$$

we have a Hopf bifurcation point. When e is greater than this value, we expect oscillations in time to occur.

Perturbed FHN

For system (2.9) the conditions for a Turing bifurcation are given by

1. $f_u + g_v + D_{11} + D_{21} < 0 \implies (2a + 3b - (a+1)\frac{1+a+\sqrt{(1-a)^2-4b}}{2} + (D_{11} + D_{21})) < e$

2. $f_u g_v + f_u D_{21} + D_{11} g_v + D_{11} D_{21} - f_v g_u > 0 \implies$

$$-e(2a + 3b - (a+1)\frac{1+a+\sqrt{(1-a)^2-4b}}{2})$$

$$-be + D_{21}(2a + 3b - (a+1)\frac{1+a+\sqrt{(1-a)^2-4b}}{2}) - D_{11}e + D_{11}D_{21} > 0$$

3. $(f_u D_v + D_{11} D_v + g_v D_u + D_{21} D_u) > 0 \implies$

$$D_v/D_u > \frac{e + D_{21}}{(2a + 3b - (a+1)\frac{1+a+\sqrt{(1-a)^2-4b}}{2}) + D_{11}}$$

4. $(f_u D_v + D_{11} D_v + g_v D_u + D_{21} D_u)^2 > 4 D_u D_v (f_u g_v + f_u D_{21} + D_{11} g_v + D_{11} D_{21} - f_v g_u) \implies$

$$[D_v D_u - D_u \frac{e + D_{21}}{(2a + 3b - (a+1)\frac{1+a+\sqrt{(1-a)^2-4b}}{2}) + D_{11}}]^2 >$$

$$4 D_u D_v (-e(2a + 3b - (a+1)\frac{1 + a + \sqrt{(1-a)^2 - 4b}}{2}))$$

$$be + D_{21}(2a + 3b - (a+1)\frac{1 + a + \sqrt{(1-a)^2 - 4b}}{2}) - D_{11}e + D_{11}D_{21}$$

Solving condition 4 first we define

$$s = D_u \frac{e + D_{21}}{(2a + 3b - (a+1)\frac{1+a+\sqrt{(1-a)^2-4b}}{2}) + D_{11}}$$

then define

$$p = be + D_{21}(2a + 3b - (a+1)\frac{1 + a + \sqrt{(1-a)^2 - 4b}}{2}) - D_{11}e + D_{11}D_{21}$$

Plugging into condition 4 we are left with the the following quadratic in d_c to solve

$$d_c^2 + d_c(2s - 4p) + s^2 = 0,$$

recall d_c is our diffusion ratio.

We can solve to find the critical diffusion bifurcation point

$$d_c = \frac{4p - 2s + \sqrt{[2s - 4p]^2 - 4s^2}}{2}.$$

Note clearly that this critical diffusion point is much more complicated than the bifurcation point derived for the DFHN due to the additional perturbation added in the system. Comparing the 4 conditions of the DFHN and the PFHN we see that in the PFHN model the conditions include additional forcing terms either adding or taking away from an expression. This means that there will be added constraints on parameters in order to induce patterns. This means that the size of the parameter space will decrease in order to accommodate these extra constraints

Following the same steps as previous we reach the new conditions needed for a Hopf bifurcation.

1. $f_u g_v + f_u D_{21} + D_{11} g_v + D_{11} D_{21} - f_v g_u > 0 \implies$

$$e(2a + 3b - (a+1)\frac{1 + a + \sqrt{(1-a)^2 - 4b}}{2})$$

$$-be + D_{21}(2a + 3b - (a+1)\frac{1 + a + \sqrt{(1-a)^2 - 4b}}{2}) - D_{11}e + D_{11}D_{21} > 0$$

2. $f_u + g_v + D_{11} + D_{21} = 0 \implies$

$$e = 2a + 3b - (a+1)\frac{1 + a + \sqrt{(1-a)^2 - 4b}}{2} + (D_{11}D_{21})$$

3. Note from the general theory of section 2 we noted that condtion 3 of a Hopf bifurcation will stay the same as in the deterministic setting as all that we have added on is a constant so when we differentiate it makes no difference.

Given all these conditions hold we find that at

$$e = 2a + 3b - (a+1)\frac{1 + a + \sqrt{(1-a)^2 - 4b}}{2} + (D_{11}D_{21}),$$

we have a Hopf bifurcation point. Comparing the Hopf bifurcation points for the FHN and the PFHN we notice they are nearly identical points however when the perturbation we notice we have the new additional forcing terms present. This implies that in the PFHN model we would have to increase the size of e in order to accommodate for the forcing terms. Showing that also in system (2.3) the Hopf bifurcation will occur sooner than in the perturbed setting.

3.3.2 Brusselator model

In this section we shall use the conditions (3.8) and (3.17) to investigate the Bru and the PBru to investigate what constraints need to be on the parameters in the model in order for patterns to appear.

Deterministic Bru

Recalling the system (2.4) we look for a spatially homogenous steady state we set

$$a - (b+1)u + u^2v = 0, \ \ bu - u^2v = 0$$

solving we these equations we find our steady state to be

$$(u_s, v_s) = (a, b/a).$$

Following the notation described in equation (3.2) we find that

$$f_u = b - 1, f_v = a^2, g_u = -b, g_v = -a^2. \tag{3.20}$$

Then using the DDI conditions we derived (3.8) we can see what conditions have to be satisfied in order for patterns to occur in the Brusselator model

1. $f_u + g_v < 0 \implies$

$$b < 1 + a^2$$

We can see that this condition places a constraint on the size of our parameter b

2. $f_u g_v - f_v g_u > 0 \implies$

$$a^2 > 0$$

3. $D_v f_u + D_u g_v > 0 \implies$

$$\frac{D_v}{D_u} > \frac{a^2}{b-1}$$

. From this condition we can see that $b > 1$ to ensure a positive diffusion ratio.

4. $(D_u g_v + D_v f_u)^2 > 4 D_u D_v (f_u g_v - f_v g_u) \implies$

$$(D_v(b-1) - D_u a^2)^2 > 4 D_v D_u a^2$$

We can solve condition 4 using (3.19) to find the specific point where the steady state will become unstable and we will see patterns begin to appear

$$d_c = \frac{2a^2(b-1) + 4a^2 + \sqrt{[4a^2 - 2a^2(b-1)]^2 - 4a^4(b-1)^2}}{2(b-1)^2}, \quad \text{where } d_c = D_v/D_u$$

When running numerical simulations we will be able to compare the theoretical results and see if diffusion ratios below this value do not generate patterns. However this result provides us a theoretical value for at which diffusion ratio patterns are induced

Following the general formulation from above we know the eigenvalues tale the form of (3.7). Here we are checking the conditions for a Hopf bifurcation. So the trace and determinant are (3.9) From the conditions we have derived for a Hopf bifurcation we have

1. $f_u g_v - f_v g_u > 0 \implies a^2 > 0$

   Satisfied from Turing and the fact all parameters in the model are positive

2. $f_u + g_v = 0 \implies b = 1 + a^2$

3. For this particular model we see the real part of the eigenvalue is

$$\alpha(b) = b - 1 - a^2$$

   we see $\alpha'(b) = 1 \neq 0$

' Hence given all conditions are satisfied showing that at

$$b = 1 + a^2,$$

we have a Hopf bifurcation and when b is greater than this value is when we expect oscillations in time to occur.

Perturbed Bru

Considering (2.10) the system. Now looking at the conditions for a Turing bifurcation are given by

1. $f_u + g_v + D_{11} + D_{21} < 0 \implies$

$$b < 1 + a^2 - (D_{11} + D_{21})$$

2. $f_u g_v + f_u D_{21} + D_{11} g_v + D_{11} D_{21} - f_v g_u > 0 \implies$

$$b > D_{11} a^2 - a^2 - D_{21} - D_{11} D_{21}$$

3. $(f_u D_v + D_{11} D_v + g_v D_u + D_{21} D_u) > 0 \implies$

$$\frac{D_v}{D_u} > \frac{a^2 - D_{21}}{b - 1 - D_{21}}$$

4. $(f_u D_v + D_{11} D_v + g_v D_u + D_{21} D_u)^2 > 4 D_u D_v (f_u g_v + f_u D_{21} + D_{11} g_v + D_{11} D_{21} - f_v g_u) \implies$

$$\left(D_v - \frac{D_u a^2 + D_{v_2}}{b - 1 - D_{v_2}}\right)^2 > 4 D_u D_v (b - D_{11} a^2 + a^2 + D_{21} + D_{11} D_{21})$$

We can see with the extra terms we now have more constraints on our parameters, this does mean that we are likely to end up with a larger parameter space where patterns can exist depending on the size of the perturbation terms. In the deterministic setting condition two was automatically satisfied where as now it provides a constraint for the parameter b. condition b now requires $b + D_{21} > 1$ and that $a^2 > D_{21}$ which will ensure the diffusion ratio is positive. We also see the effect of the perturbation in condition 1, in the deterministic setting $b < 1 + a^2$ where as here $b < 1 + a^2 - (D_{11} + D_{21})$ due to this subtraction of the perturbation terms we could assume that the value of b would have to reduce in order to induce patterns, hence we can imply a changing parameter region as a result of an added perturbation.

Solving condition 4 first we define

$$s = \frac{a^2 + D_{21}}{b - 1 - D_{21}},$$

then define

$$p = (b - D_{11} a^2 + a^2 + D_{21} + D_{11} D_{21}),$$

so in order to solve $d_c^2 + d_c(2s - 4p) + s^2 = 0$ recall d is our diffusion ratio. We can solve to find that the critical diffusion bifurcation point is once again when we numerically

simulate these models it will be interesting to see how the parameter spaces change and to see whether the size of the critical diffusion ratio has gone up or down

$$d_c = \frac{4p - 2t + \sqrt{[2t - 4p]^2 - 4t^2 - 4a^2}}{2}.$$

Comparing the two sets of conditions we have derived for the PBru and the Bru one obvious difference is that condition 2 is no longer satisfied automatically in the PBru system this is itself demonstrates how in the DBru we could have a parameter spaces that satisfies the conditions and induces patterns however in the PBru this specific parameter space would not be sufficient. Another clear difference is the condition 3 was satisfied by requiring $b > 1$ however in the PBru we now have conditions on both a and b which ensure the diffusion ratio is positive. This shows the effects of the extra perturbation when added to the system.

Following the same steps as above we reach the new conditons needed for a Hopf bifurcation.

1. $f_u g_v + f_u D_{21} + D_{11} g_v + D_{11} D_{21} - f_v g_u > 0 \implies$

$$b > D_{11} a^2 - a^2 - D_{21} - D_{11} D_{21}.$$

   Which is satisfied given the conditions on the Turing Patterns

2. $f_u + g_v + D_{11} + D_{21} = 0 \implies$

$$b = 1 + a^2 - (D_{11} + D_{21}),$$

   recall can't happen if condition 1 of DDI holds.

3. Note from the general theory of section 2 we noted that condtion 3 of a Hopf bifurcation will stay the same as in the deterministic setting as all that we have added on is a constant so when we differentiate it makes no difference.

Hence,

$$b = 1 + a^2 - (D_{11} + D_{21}),$$

is a Hopf bifurcation point. Once again comparing the two Hopf bifurcation points that we have derived for the Bru and PBru respectively we see that the PBru has additional terms taking away from the parameter b this implies that if the conditions hold to induce a Hopf bifurcation the size of the parameter b would have to be larger in the PBru than in the Bru.

3.3.3 Schnakenberg model

In this section we shall use the conditions (3.8) and (3.18) to investigate the Sch and the PSch to investigate what constraints need to be on the parameters in the model in order for patterns to appear.

Deterministic Sch

Recalling the system (2.5) we look for a spatially homogenous steady state we set

$$a - u + u^2 v = 0 \ \ b - u^2 v = 0$$

Solving we these equations we find our steady state to be

$$(u_s, v_s) = (a + b, \frac{b}{(a+b)^2}).$$

Following the notation described in equation (3.2) we find that

$$f_u = \frac{b-a}{a+b}, f_v = (a+b)^2, g_u = \frac{-2b}{a+b}, g_v = -(a+b)^2. \tag{3.21}$$

Then using the DDI conditions we derived (3.8) we can see what conditions have to be satisfied in order for patterns to occur in the Schnakenberg model.

To make the analysis easier we make the transformation and set

$$b - a = \alpha, a + b = \beta$$

which means

$$a = \frac{\beta - \alpha}{2}, b = \frac{\beta + \alpha}{2}$$

Looking at the conditions for a Turing bifurcation

1. $f_u + g_v < 0 \implies$
$$b - a < (a+b)^3 \implies \alpha < \beta^3$$

2. $f_u g_v - f_v g_u > 0 \implies$
$$(a+b)^2 > 0 \implies \beta^2 > 0$$

3. $D_v f_u + D_u g_v > 0 \implies$
$$\frac{D_v}{D_u} > \frac{(a+b)^3}{b-a} \implies \frac{D_v}{D_u} > \frac{\beta^3}{\alpha}$$
   We see that we require $b > a$ to ensure a positive diffusion coefficient.

4. $(D_u g_v + D_v f_u)^2 > 4 D_u D_V (f_u g_v - f_v g_u) \implies$
$$(D_v(b-a) - D_u(a+b)^3)^2 > 4 D_u D_v (a+b)^4 \implies (D_v \alpha - D_u \beta^3)^2 > 4 D_u D_v \beta^4$$

Solving condition 4 using (3.19) we are able to find the bifurcation point at which the steady state becomes unstable we find that

$$d_c = \frac{2\alpha\beta^3 + 4\beta^4 + \sqrt{[2\alpha\beta + 4\beta^4]^2 - 4\alpha^2\beta^6}}{2\alpha^2}.$$

27

When plugging in parameter values which ever value is positive we take to be the critical bifurcation point at which point any value greater than this we would expect patterns to appear.

Following the general formulation from above we know the eigenvalues tale the form of (3.8). Here we are checking the conditions for a Hopf bifurcation hence the leading wavenumber here is k=0. So the trace and determinant have are (3.9) From the conditions wehave derived for a Hopf bifurcation we have

1. $f_u g_v - f_v g_u > 0 \implies (a+b)^2 > 0 \implies \beta^2 > 0$. This is satisfied automatically as all parameters are positive.

2. $f_u + g_v = 0 \implies b - a = (a+b)^3 \implies \alpha = \beta^3$.

3. Here we see the real part of our eigenvalue is $\alpha(\alpha) = \frac{\alpha}{\beta} - \beta^2$ when we differentiate this we get $\alpha' = \frac{1}{\beta}$ which we see is non zero

Hence given all conditions are satisfied showing that at $\alpha = \beta^3$ we have a Hopf bifurcation and when α is greater than this value is when we expect oscillations in time to occur.

Perturbed version

For system (2.11) the conditions for a Turing bifurcation are given by

1. $f_u + g_v + D_{11} + D_{21} < 0 \implies$

$$(a+b)^3 > (a+b)(D_{11} + D_{21}) + (b-a) \implies \beta^3 > \beta(D_{11} + D_{21}) + \alpha$$

2. $f_u g_v + f_u D_{21} + D_{11} g_v + D_{11} D_{21} - f_v g_u > 0 \implies$

$$(a+b)^3 < \frac{D_{21}(b-a) + D_{11}D_{21}(a+b)}{D_{11} - 1} \implies \beta^3 < \frac{D_{21}\alpha + D_{11}D_{21}\beta}{D_{11} - 1}$$

3. $(f_u D_3 + D_{11}D_v + g_v D_u + D_{21}D_u) > 0 \implies$

$$\frac{D_v}{D_u} > \frac{(a+b)^3}{(b-a) + D_{11} - 1} \implies \frac{D_v}{D_u} > \frac{\beta^3}{\alpha + D_{11}\beta}$$

4. $(f_u D_v + D_{11}D_v + g_v D_u + D_{21}D_u)^2 > 4D_u D_v(f_u g_v + f_u D_{21} + D_{11}g_v + D_{11}D_{21} - f_v g_u) \implies$

$$[D_v - \frac{D_u \beta^3}{\alpha + D_{11}\beta}]^2 > 4D_u D_v(\beta^3 + D_{21}\alpha - D_{11}(\beta + \alpha) + D_{11}D_{21})$$

28

Solving condition 4 first we define

$$t = \frac{\beta^3}{\alpha + D_{11}\beta},$$

then define

$$p = (\beta^3 + D_{21}\alpha - D_{11}(\beta + \alpha) + D_{11}D_{21}),$$

so in order to solve $d^2 + d(2s - 4t) + s^2 = 0$ recall d is our diffusion ratio. We can solve to find that the critical diffusion bifurcation point is once again when we numerically simulate these models it will be interesting to see how the parameter spaces change and to see whether the size of the critical diffusion ratio has gone up or down

$$d_c = \frac{4p - 2s + \sqrt{[2s - 4p]^2 - 4s^2}}{2}.$$

Once again we see when we compare the conditions for the Sch and the PSch like in the Bru and PBru system condition 2 that was automatically satisfied before now has a condition placed on it. As is the same for condition 3 which ensures a positive diffusion parameter. In this case I feel the conclusions are the same that with these extra constraints we can expect a larger parameter region in order to accomadate for the extra perturbation terms.

Now looking at the conditions needed to get a Hopf bifurcation

1. $f_u g_v + f_u D_{21} + D_{11}g_v + D_{11}D_{21} - f_v g_u > 0 \implies$

$$\beta^3 < \frac{D_{21}\alpha D_{11}D_{21}\beta}{D_{11} - 1},$$

2. $f_u + g_v + D_{11} + D_{21} = 0 \implies$

$$\beta^3 = \beta(D_{11} + D_{21}) + \alpha,$$

3. Note from the general theory of section 2 we noted that condtion 3 of a Hopf bifurcation will stay the same as in the deterministic setting as all that we have added on is a constant so when we differentiate it makes no difference.

Hence given all the conditions of a Hopf bifurcation are satisfied we can say that at

$$\beta^3 - \beta(D_{11} + D_{21}) = \alpha,$$

we have a Hopf bifurcation. Comparing our two Hopf bifurcation points from the conditions that we have derived we see that actually we get some interesting results where as in previous models we expect the bifurcation parameter to be larger when the system is perturbed we see in the PSch that the Hopf bifurcation point gains additional terms from the perturbation meaning that we would have to decrease the parameter or keep it the same size in order would the Hopf bifurcation to be induced.

3.4 Chemotaxis

In this section we shall look at the systems of chemotaxis that we intriduced in Chapter 2. First we shall derive analytical conditions for which we expect patterns to occur for the general systems (2.16) and (2.17). Then we shall apply these conditions for specific examples.

3.4.1 Deterministic Chemotactic Patterning

To analyse the stability of spatially homogeneous steady states for chemotaxis system (2.16) we linearise about the steady state

$$U = u - u_s, \quad V = v - v_s.$$

To obtain

$$\frac{\partial U}{\partial t} = D_u \Delta U - \chi u_s \Delta v + f_u U,$$
$$\frac{\partial v}{\partial t} = D_v \Delta v + g_u U + g_v V \tag{3.22}$$

With the same homogeneous Neumann initial and boundary conditions (2.2)

Then as before we are looking for solutions of the form given in (3.1), we obtain

$$\frac{d}{dt} \begin{bmatrix} \bar{U} \\ \bar{V} \end{bmatrix} A \begin{bmatrix} \bar{U} \\ \bar{V} \end{bmatrix}, \quad \text{where } A = \begin{bmatrix} f_u - D_u k^2 & \chi u_s k^2 \\ g_u & g_v - D_v k^2 \end{bmatrix} \tag{3.23}$$

Comparing the stability matrix to the one derived in (3.4) we see that the A_{12} entry has changed due to the general model having no f_v and that we will get an extra to the k^2 terms which will play a part when looking at unstable perturbations.

The characteristic equation is given by

$$\lambda^2 - Tr(A)\lambda + \delta(k^2) = 0.$$

The eigenvalues are given by

$$\lambda = \frac{1}{2}(Tr(A) \pm \sqrt{Tr^2(A) - 4\delta(k^2)} \tag{3.24}$$

where

$$Tr(A) = (f_u + g_v) - (D_u + D_v)k^2, \tag{3.25}$$
$$Det(A) = \delta(k^2) = D_u D_v k^4 - (D_u g_v + D_v f_u + \chi u_s g_u)k^2 + f_u g_v. \tag{3.26}$$

30

Recall when looking for the Hopf Bifurcation we choose the leading wavenumber of the solution to be k=0. Hence this then makes

$$Tr(A) = (f_u + g_v), \tag{3.27}$$
$$Det(A) = \delta(0) = f_u g_v. \tag{3.28}$$

We note that in the chemotactic setting the determinant is reduced massively which will help us when determining conditions for which patterns can occur.

For the steady state (u_s, v_s) to be stable to a spatially homogeneous perturbation we require

$$Tr(A) < 0, k = 0 \iff f_u + g_v < 0 \text{ (C1)}$$

&

$$Det(A) > 0, k = 0 \iff f_u g_v > 0 \text{ (C2)}$$

Now for condition 2, $Tr(A)$ can't be greater than zero as from (C1) as $Tr(A) = (f_u + g_v) - (D_u + D_v)k^2 < 0 \ \forall k$.

Thus can obtain patterning if there are some positive values of k^2 for which $\delta(k^2) = Det(A) < 0$. Solving $\delta(k^2)$ to find the smallest positive root k_{min}^2 and plugging that value in to find δ_{min}, we get

$$
\begin{aligned}
k_{min}^2 &= \frac{D_u g_v + D_v f_u + \chi u_s g_u}{2 D_u D_v} \\
\delta_{min} &= f_u g_v - \frac{(D_u g_v + D_v f_u + \chi u_s g_u)^2}{4 D_u D_v}
\end{aligned}
\tag{3.29}
$$

Thus $\delta(k^2) < 0$ for some $k^2 > 0 \iff$

$$k_{min}^2 \iff D_u g_v + D_v f_u + \chi u_s g_u > 0 \text{ (C3)}$$

&

$$\delta_{min} < 0 \iff (D_u g_v + D_v f_u + \chi u_s g_u)^2 > 4 D_u D_v f_u g_v \text{ (C4)}$$

Putting all the conditions together we get

$$
\begin{aligned}
Tr(A) < 0, k = 0 &\iff f_u + g_v < 0 \text{ (C1)} \\
Det(A) > 0, k = 0 &\iff f_u g_v > 0 \text{(C2)} \\
k_{min}^2 > 0 &\iff D_u g_v + D_v f_u + \chi u_s g_u > 0 \text{ (C3)} \\
\delta_{min} < 0 &\iff (D_u g_v + D_v f_u + \chi u_s g_u)^2 > 4 D_u D_v f_u g_v \text{ (C4)}
\end{aligned}
\tag{3.30}
$$

(3.30) form our complete set of conditions which have to be satisfied for chemotactic driven instability. We will be able to find a point at which the chemotactic sensitivity $\chi*$ if $\chi > \chi*$ then the steady state will become unstable and we would expect patterns to appear. As you can see from the conditions in chemotaxis system the chemotactic sensitivity coefficient play important role and here the instability is driven by the interplay between diffusion and chemotaxis.

Conditions for the Hopf bifurcation are as follows:

$$
\begin{aligned}
\beta(\mu_0) \neq 0 &\implies f_u g_v > 0 \\
\alpha(\mu_0) = 0 &\implies f_u + g_v = 0 \\
\frac{d(f_u + g_v)}{d\mu}(\mu_0) &\neq 0
\end{aligned}
\tag{3.31}
$$

where μ is an arbitary bifurcation parameter of a given system.

3.4.2 Perturbed Chemotactic Patterning

Linearising the system as in (2.17)

$$
\begin{aligned}
\frac{\partial U}{\partial t} &= D_u \Delta u - \chi u_s \Delta v + f_u U + D_{11} U, \\
\frac{\partial V}{\partial t} &= D_v \Delta V + g_u U + g_v V + D_{21} V
\end{aligned}
\tag{3.32}
$$

Considering solutions of (3.32) of the form (3.3) we obtain

$$
\frac{d}{dt}\begin{bmatrix} \bar{U} \\ \bar{V} \end{bmatrix} = A \begin{bmatrix} \bar{U} \\ \bar{V} \end{bmatrix}, \text{ where } A = \begin{bmatrix} f_u + D_{11} - D_u k^2 & \chi u_s k^2 \\ g_u & g_v + D_{21} - D_v k^2 \end{bmatrix}
\tag{3.33}
$$

Note we have the exactly same stability matrix as in (3.23) just with the extra forcing terms which we described in (3.12).

The eigenvalues of matrix A in (3.33) are given by (3.24) with

$$
\begin{aligned}
Tr(A) &= (f_u + g_v + D_{11} + D_{21}) - (D_u + D_v)k^2, \\
Det(A) = \delta(k^2) &= D_u D_v k^4 - (D_u g_v + D_v f_u + D_{11} D_v + D_u D_{21} + \chi \\
& u_s g_u)k^2 + f_u g_v + f_u D_{21} + D_{11} g_v + D_{11} D_{21}.
\end{aligned}
\tag{3.34}
$$

Going back to the conditions required on the steady state in order for patterns to appear, we have

$$
Tr(A) < 0, k = 0 \iff (f_u + g_v + D_{11} + D_{21}) < 0 \text{ (CS1)}
$$

&

$$Det(A) > 0, k = 0 \iff f_u g_v + f_u D_{21} + D_{11} g_v + D_{11} D_{21} > 0 \ (\text{CS2})$$

and $\delta(k^2) = Det(A) < 0$ for $k^2 > 0$.

Solving $\delta(k^2)$ to find the smallest positive root k^2_{min} and plugging that value in to find δ_{min}, we get

$$k^2_{min} = \frac{D_u g_v + D_v f_u + D_{11} D_v + D_u D_{21} + \chi u_s g_u}{2 D_u D_v}$$

$$\delta_{min} = f_u g_v + f_u D_{21} + D_{11} g_v + D_{11} D_{21} - \frac{(D_u g_v + D_v f_u + D_{11} D_v + D_u D_{21} + \chi u_s g_u)^2}{4 D_u D_v}$$

(3.35)

Thus $\delta(k^2) < 0$ for some $k^2 > 0 \iff$

$$k^2_{min} \iff D_u g_v + D_v f_u + D_{11} D_v + D_u D_{21} + \chi u_s g_u > 0 \ (\text{CS3})$$

&

$$\delta_{min} < 0 \iff (D_u g_v + D_v f_u + D_{11} D_v + D_u D_{21} + \chi u_s g_u)^2 >$$
$$4 D_u D_v (f_u g_v + f_u D_{21} + D_{11} g_v + D_{11} D_{21}) \ (\text{CS4})$$

Hence we can form a complete set of conditions for which we expect chemotactic patterning to occur
(CS1),(CS2),(CS3),(CS4) form our complete set of conditions which have to be satisfied for pattern formation in the chemotaxis system (2.20)

Recall when looking for the Hopf Bifurcation the leading wavenumber of the solution is k=0. Hence this then makes

$$Tr(A) = (f_u + g_v + D_{11} + D_{21}),$$
$$Det(A) = P(0) = f_u g_v + f_u D_{21} + D_{11} g_v + D_{11} D_{21}.$$

(3.36)

The conditions are as follows

$$\beta(\mu_0) \neq 0 \implies f_u g_v + f_u D_{21} + D_{11} g_v + D_{11} D_{21} > 0$$
$$\alpha(\mu_0) = 0 \implies (f_u + g_v + D_{11} + D_{21}) = 0$$
$$\frac{d\alpha}{d\mu}(\mu_0) \neq 0 \implies \frac{d(f_u + g_v + D_{11} + D_{21})}{d\mu}(\mu_0) \neq 0$$

(3.37)

Note D_{11}, D_{21} are additional constants that are present from the linerisation of the random variable in the initial model equations, when we differentiate them they go to zero. Hence if condition 3 is satisfied in the deterministic setting it will also be satisfied in the stochastic setting for the noise specified in this setting.

3.4.3 Deterministic (Dd)

Recalling system (2.19) we look for a non-trival steady state of the model we need to satisfy

$$f(u_s) \iff ru_s(1 - u_s) = 0 \implies u_s = 1.$$

We also need

$$g(u_s, v_s) = 0 \iff au_s = bv_s.$$

The non-trival steady state we find is

$$(u_s, v_s) = (1, a/b).$$

Evaluating derivatives at the steady state as before we find

$$f_u = -r, g_u = a, g_v = -b.$$

Now subbing into conditions (3.30) we get

1. $f_u + g_v < 0 \implies$

$$-r - b < 0$$

   We see that this is satisfied automatically, from the parameters been positive

2. $f_u g_v > 0 \implies$

$$rb > 0$$

   We see this condition is also automatically satisfied.

3. $D_v f_u + D_u g_v + \chi u_s g_u > 0 \implies$

$$\chi > \frac{1}{a}(rD_v + bD_u)$$

   This provides us a condition for for how big the chemotactic sensitivity has to be in order for aggregation in the model to occur.

4. $(D_v f_u + D_u g_v + \chi u_s g_u)^2 > 4D_u D_v f_u g_v \implies$

$$(\frac{\chi a}{D_u} - rd - b)^2 > 4rdb, \ d = \frac{D_v}{D_u}$$

   We can solve for the chemotactic sensitivity to get a new condition for how big χ has to be.

$$\chi > \frac{D_u}{a}(rd + b + 2\sqrt{rdb}) \text{ where } d = \frac{D_v}{D_u}.$$

From this we can see that given a value of $\chi > \chi*$, where $\chi* = \frac{D_u}{a}(rd + b + 2\sqrt{rdb})$ hence any value greater than this we expect the steady state to become unstable and patterns will begin to appear from this we can conclude $\chi*$ is our Turing bifurcation point. Provided the chemotactic sensitivity, χ and rate of production of chemoattractant, a are sufficiently strong, we can expect aggregation patterns to form.

Looking for a Hopf Bifurcation we can use the conditions (3.31)

1. $f_u g_v > 0 \implies$
$$rb > 0$$
. This is satisfied automatically due the parameters been positive.

2. $f_u + g_v = 0 \implies$
$$r = -b$$

3. $\frac{d(f_u + g_v)}{d\mu}(\mu_0) \neq 0 \implies$
$$\frac{d(-r - b)}{dr} = -1 \neq 0.$$

At $r = -b$ we can define a Hopf bifurcation. We see that this is biologically not possible since $r, b > 0$. Hence, it is not possible to have a Hopf bifurcation in the system.

3.4.4 Perturbed (Dd)

Recalling the system (2.20) along with the deterministic steady state of Dd. Now looking at the conditions (CS1-CS4) for bifurcation.

1. $(f_u + g_v + D_{11} + D_{21}) < 0 \implies$
$$r + b > D_{21} + D_{41}.$$

2. $f_u g_v + f_u D_{21} + D_{11} g_v + D_{11} D_{21} > 0 \implies$
$$rb - rD_{21} - bD_{11} + D_{11} D_{21} > 0$$
.

3. $D_u g_v + D_v f_u + D_{11} D_v + D_u D_{21} + \chi u_s g_u > 0 \implies$
$$\chi > \frac{1}{a}(bD_u + rD_v - D_{11} D_v - D_u D_{21})$$
.

4. $(D_u g_v + D_v f_u + D_{11} D_v + D_u D_{21} + \chi u_s g_u)^2 > 4 D_u D_v (f_u g_v + f_u D_{21} + D_{11} g_v + D_{11} D_{21}) \implies$

$$\chi > \frac{1}{a}(b D_u + r D_v - D_{11} D_v - D_u D_{21} + 2 D_u D_v \sqrt{rb - r D_{21} - b D_{11} + D_{11} D_{21}})$$

From this we can see that given a value of $\chi > \chi*$, where $\chi* = \frac{1}{a}(b D_u + r D_v - D_{11} D_v - D_u D_{21} + 2 D_u D_v \sqrt{rb - r D_{21} - b D_{11} + D_{11} D_{21}})$ hence any value greater than this we expect the steady state to become unstable and patterns will begin to appear from this we can conclude $\chi*$ is our Turing bifurcation point. However note that been in the perturbation setting does mean that we have extra terms contributing to the constraints hence we may find that for a given noise the bifurcation points value may either increase or decrease.

We can see that comparing CS1 to C1 to the deterministic case there is now a higher lower bound on the value of $r + b$ and this lower bound is controlled by the size of our noise term. Also comparing CS2 to C2 before this condition was automatically satisfied now it is not. It depends once again on the size of our perturbation terms.

We can investigate the Hopf bifurcation point using conditions (3.37)

1. $f_u g_v + f_u D_{21} + D_{11} g_v + D_{11} D_{21} > 0 \implies$

$$rb - r D_{21} - b D_{11} + D_{11} D_{21} > 0$$

.

2. $f_u + g_v + D_{11} + D_{21} = 0 \implies$

$$r = -b + D_{11} + D_{21}$$

3. $\frac{d(f_u + g_v + D_{11} + D_{21})}{d\mu}(\mu_0) \neq 0 \implies$

$$\frac{d(-r - b + D_{11} + D_{21})}{dr} = -1 \neq 0.$$

We can see that all three conditions can be satisfied, hence at

$$r = -b + D_{11} + D_{21}.$$

we have a Hopf bifurcation. Here we see that this point now has these additional forcing terms included in the point hence we expect that in this setting the size of the parameter r would have to increase in order to accommodate for the additional perturbation terms. Hence it may now be possible to have a Hopf bifurcation in the system.

Chapter 4

Numerical Simulations

We will now simulate the models that we have analysed theoretically. We will begin by giving an introduction to the scheme that will be used to simulate the reaction diffusion and chemotaxis systems.

4.1 Numerical schemes

We shall first detail the two numerical schemes that we use to run the simulations first talking about the finite difference scheme used to run my deterministic simulations, models (2.3,2.4,2.5). Then I will talk about how I use the same scheme to simulate the stochastic versions of the models (2.13,2.14,2.15)

4.1.1 Finite difference scheme Deterministic

We are dealing with a rectangular spatial domain we must discretise each dimension of $[a, b] \times [c, d]$. Suppose we discretise the x dimension into I intervals and the y dimension into J intervals. Now the spatial distances between nodes in the x and y dimensions are given by $h_x = \frac{b-a}{I}$ and $h_y = \frac{d-c}{J}$. The result of this discretisation is now a 2-dimensional grid of nodes (x_i, y_j) where $x_i = a + ih_x$ for $i \in \{0, ..., I\}$ and $y_j = c + jh_y$ for $j \in \{0, ..., J\}$. The discretisation of time into N steps is carried out in exactly the same way as in the previous section, with $\tau = \frac{T}{N}$ and $t_n = \tau n$ for $n \in \{1, ..., N\}$. For a triple (x_i, y_j, t_n) of these discrete points we denote $u(x_i, y_j, t_n) = u_{i,j}^n$.

The Laplacian of u or v on the interior grid nodes can now be approximated via centred finite differences:

$$\Delta u(x_i, y_j, t_n) \approx \frac{u_{i-1,j}^n - 2u_{i,j}^n + u_{i+1,j}^n}{h_x^2} + \frac{u_{i,j-1}^n - 2u_{i,j}^n + u_{i,j+1}^n}{h_y^2},$$

for $i \in \{1, ..., I-1\}$ and $j \in \{1, ..., J-1\}$.

We approximate the time derivative as

$$\frac{\partial u(x_i, y_j, t_n)}{\partial t} \approx \frac{u_{i,j}^{n+1} - u_{i,j}^n}{\tau}.$$

4.1.2 Finite difference scheme Stochastic

Now we can extend the finite difference scheme above to the stochastic setting in order to do this we need to know how to approximate sample paths of the Q-Wiener process using Theorem 2.81 [**30**]. Using given eigenfunctions, γ_i and eigenvalues q_i needed for the formula given in Theorem 2.81 we are able to create sample paths of the Q-Wiener process through

$$W^I(t_{n+1}) - W^I(t_n) = \sqrt{\tau} \sum_{i=1}^{I} \sqrt{q_i} \gamma_i \zeta_i^n$$

where

$$\zeta_i^n = \frac{\beta_i(t_{n+1}) - \beta_i(t_n}{\sqrt{\tau}}$$

Here this means that $\zeta_i^n \sim N(0,1)$ and can be easily sampled. Note that often the eigenfunctions are trigonometric functions meaning that with careful choice of spatial points evaluation of the Q-Wiener process can be achieved through a single Fourier transform. As the eigenfunctions are trigonometric functions this allows us to split them up into their respective real and imaginary parts which we then use for the axis.

From Example 10.12 [**30**], we can make the extension to two dimensions

$$W^I(t_{n+1}) - W^I(t_n) = \sqrt{\tau} \sum_{i_1=-I_1/2+1}^{I_1/2} \sum_{i_2=-I_2/2+1}^{I_2/2} \sqrt{q_{i_1,i_2}} \gamma_{i_1,i_2} \zeta_{i_1,i_2}^n$$

where

$$\gamma_{i_1,i_2} = \frac{1}{\sqrt{a_1 a_2}} e^{2\pi i i_1 x_1/a_1} e^{2\pi i i_2 x_2/a_2}, \quad q_{i_1,i_2} = e^{-\alpha \lambda_{i_1,i_2}}$$

for $i = \sqrt{-1}$, parameter $\alpha > 0$, $\lambda_{i_1,i_2} = i_1^2 + i_2^2$, for even integers I_1, I_2. a_1, a_2 are the size of the domain in the x, y directions respectively. $\zeta_{i_1,i_2}^n \sim N(0,2)$.

When we simulate the stochastic models we shall be taking an average over 100 realisations then the plot that you see will be the average of them 100 simulations.

4.2 FitzHugh-Nagumo model

For all our simulations we shall be simulating in python using the standard Numpy and Matplotlib packages. We use use a spatial domain of $x, y \in (0,1)^2$ and a time domain of $t \in (0, 15]$ where our time step $dt = 0.001$.

4.2.1 DFHN
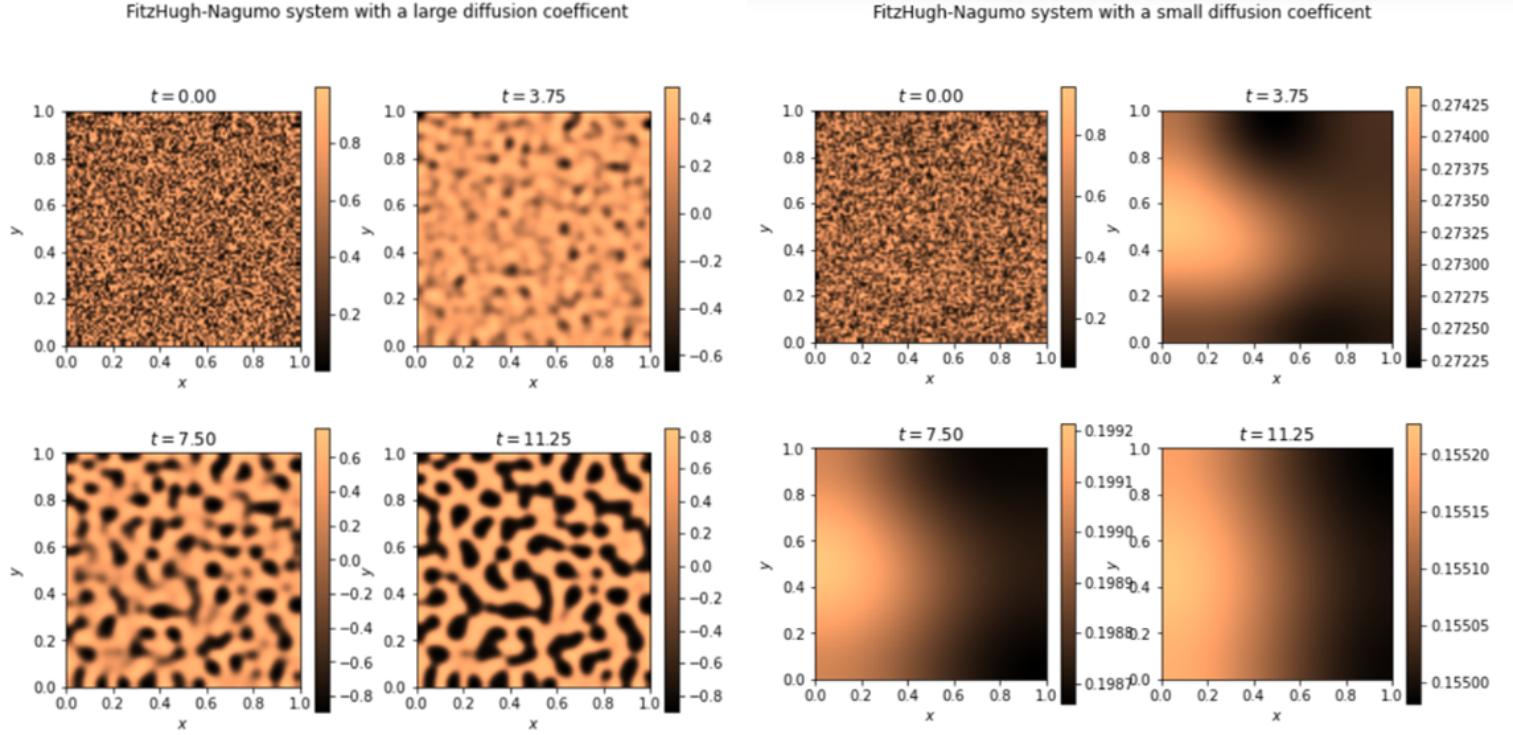
Figure 4.1: System (2.3) for parameter values $a = 3.42, b = 1.21, e = 1$. The left image $D_u = 2.8 \cdot 10^{-4}, D_v = 5.3 \cdot 10^{-3}$. The right image $D_u = 2.8 \cdot 10^{-2}, D_v = 5.3 \cdot 10^{-4}$

The conditions we have to satisfy for Turing patterns are as follows

1. $e > \frac{1}{b}(2a + 3b - (a + 1)\frac{1+a+\sqrt{(1-a)^2-4b}}{2}) \implies 1 < 0.7018$ We see this condition is satisfied also we see $f_u = 0.7018$ which is in line with our theoretical predictions.

2. $b > e \implies 1.21 > 1$

3. $\frac{D_v}{D_u} > \frac{e}{(2a+3b-(a+1)\frac{1+a+\sqrt{(1-a)^2-4b}}{2})} \implies 18.9286 > 1.4249$.

4. $(D_u g_v + D_v f_u)^2 > 4D_u D_v (f_u g_v - f_v g_u)$

   We can solve this to show that our critical Turing bifurcation point $d_c = D_v/D_u$ satisfies

$$d_c = \frac{2f_u g_v - 4f_v g_u + \sqrt{[2f_u g_v - 4f_v g_u]^2 - 4f_u^2 g_v^2}}{2f_u^2}$$

We see that the first 3 conditions have been satisfied and the forth we shall check it through working out the critical diffusivity then checking it against the value we used in our simulation.
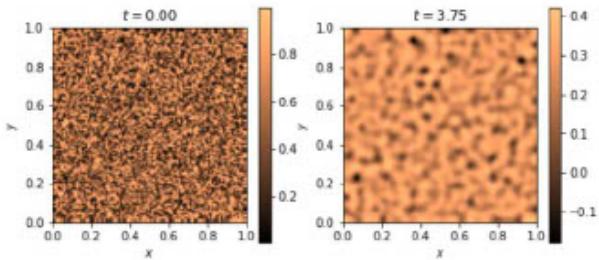
We can check the critical diffusivity value d_c this was defined above. Which for our given parameters we get a value of $d_c = 6.67286$ in our simulations of a large diffusion coefficient we use a diffusion ratio of 18.93 hence condition 4 would be satisfied hence explaining why we see spatial patterns in the simulations.

When we reduce our diffusion ratio to a value to below this given point, in the simulation on the right we use 0.01893 we see that patterns do not appear and the system appears to tend towards a homogeneous state. In conclusion we see that our theoretical results match up nicely with our simulations.
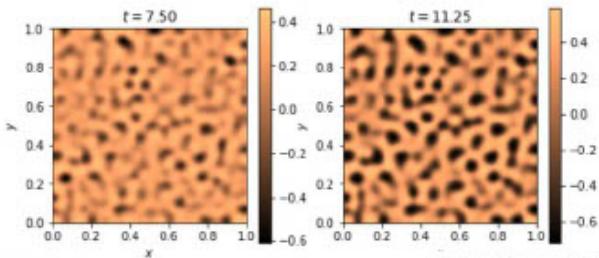
4.2.2   Stochastic simulations

We are now going to look at the effect of noise on the system (2.13). We choose diffusion parameters such that $d = D_v/D_u = 6.67$ which is exactly equal to the Turing bifurcation point determined above.
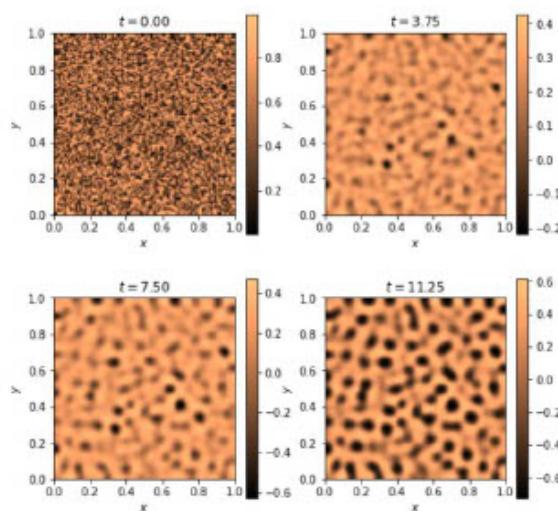
From the Top simulation in (Figure 4.2) below we see that we still establish patterns however they are much weaker than the patterns we were able to create in (Figure 4.1). As we are now on the bifurcation point we can more closely analyse the effect of noise will induce patterns.
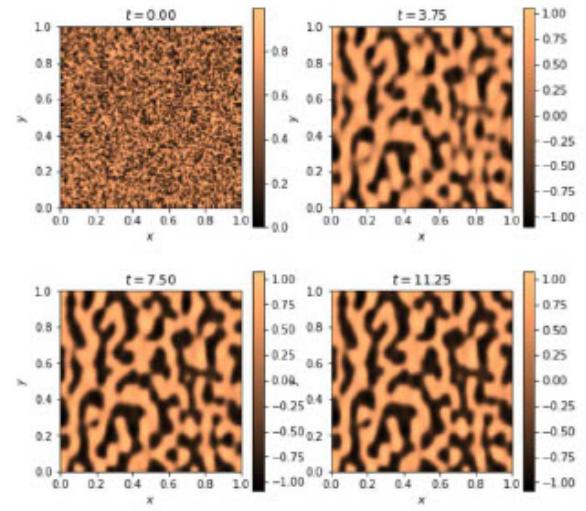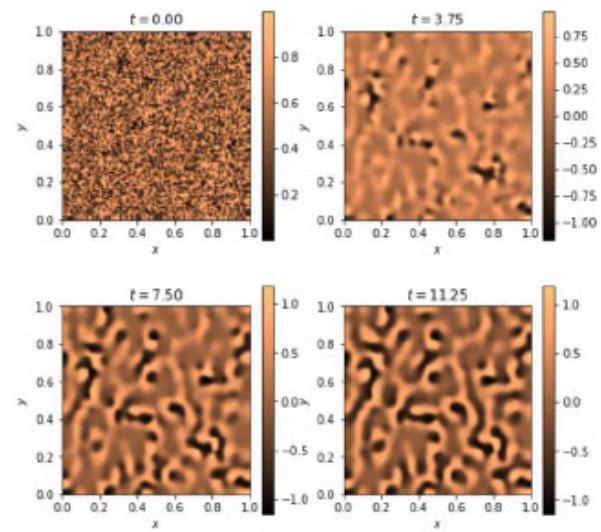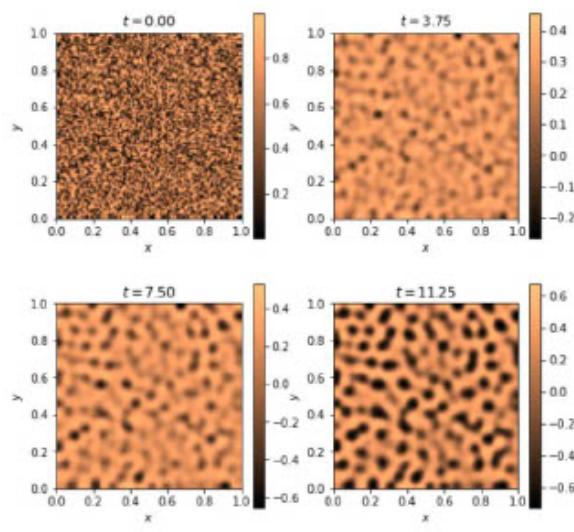
Figure 4.2: System (2.3) for parameter values $a = 3.42, b = 1.21, e = 1, D_u = 2.8 \cdot 10^{-4}, D_v = 1.8676 \cdot 10^{-3}$. Top left: $\sigma_1 = \sigma_2 = 0.005$, Top right: $\sigma_1 = \sigma_2 = 0.5$, Bottom left: $\sigma_1 = c_u u, \sigma_2 = c_v v$ where $c_u = c_v = 0.005$, Bottom right: $\sigma_1 = c_u u, \sigma_2 = c_v v$ where $c_u = c_v = 0.5$

Additive Noise

We consider the Top left and the Top right figure for this section.

Starting with small additive noise we see the effect of this is minimal as the densities of each chemical are practically identical, however comparing the top left image and the top image we do see a slight change in the positioning of the spots hence suggesting small additive noise can induce a different mode in system.

Now looking at the Top right image we a brand new pattern arrangement than what we have seen before, we see, comparing to figure 4.1 with the large diffusion coefficient, that the densities of each chemical is much more concentrated indicated by the colour bar we also see much larger groupings of the chemicals involved hence suggesting that a large additive noise can induce much stronger pattern formation similar to using a much larger diffusion coefficient.

In the SFHN model, with additive noise we see that we are able to induce different patterns into the system, when the model is around its critical diffusion bifurcation. We see that the additive noise acts in a way that is able to shift the model into selecting a different mode which in turn creates a different pattern formation.

Multiplicative Noise

Here we look at the bottom left and the bottom right images.

$c_u, c_v \in \mathbb{R}$ can be viewed as the the intensity of our multiplicative noise. We shall compare the effects of low intensity multiplicative noise to high intensity multiplicative noise. In many different articles we see that this type of noise has many different interpretations, for example some of its uses are purely computational and using this type of noise ensures that the solution will never go negative meaning that the system can keep its physical realism another interpretation of this type of noise can be viewed as the random effects by a small number of molecules in a reaction or a perturbation of a control parameter.

Looking at the bottom left image, we see that using a low intensity multiplicative noise once again induces a different mode, which can be seen by the different number and positioning of the spots. However, when we increase the intensity to we see from the simulation, bottom right image, that the system quickly becomes ruined and little patterns can occur, this is an interesting result as in the additive setting with the same intensity, we gained clear distinct patterns. This shows us clearly that when we are using multiplicative noise compared to additive different ranges of values we can use for noise intensity will exist.

In conclusion we can say that when the SFHN model is close to its critical diffusion bifurca-

tion, noise can play an essential role in inducing patterns in a system. Conversely from the bottom right image we can see that if the noise is too big it begins to play a large part in a system's dynamics it can totally ruin any patterns we are looking to achieve to the point where no real conclusions can be drawn from it. Recall from earlier that the FHN model was used famously to provide a description as to how patterns can form on animal skin, these simulations show that if this explanation is correct for animal skin pattern formation any problems during embryonic development which we could attribute as 'noise' can lead to serious developmental issues with patterns on the skin.

4.2.3 Hopf Bifurcation
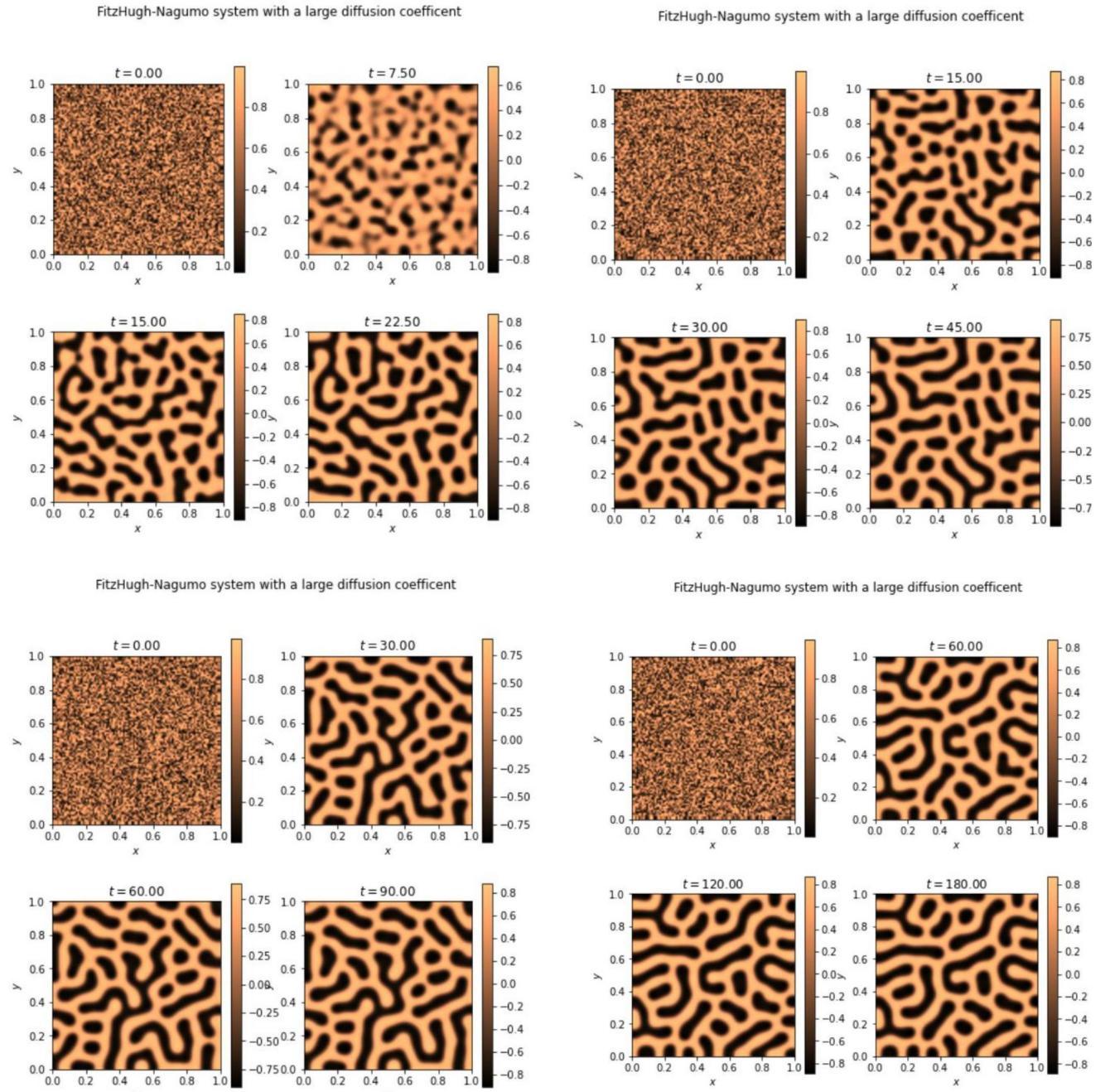
Figure 4.3: System (2.3) for parameter values $a = 3.42, b = 1.21, e = 1.03888, D_u = 2.8 \cdot 10^{-4}, D_v = 5.3 \cdot 10^{-3}$.

Theoretically we should establish the same patterns at equal time points due to the simulations been deterministic, however if we compare separate time points such as $t = 15$

and $t = 60$. Although tricky to see the oscillations we can see that there is some change in the plots between the same time points implying that our theoretical conditions for a Hopf bifurcation in the FHN model are valid. In order to investigate this properly one could take a point in space an plot a time evolution of of that space point.

4.3 Brusselator model

4.3.1 DBru

Although we have no direct applications for patterns of this model we do see that spot like patterns can be exhibited (figure 4.3) these are seen below

The conditions we have to satisfy for Turing patterns, are as follows

1. $b < 1 + a^2 \implies 7.02 < 7.25$ We see that this is satisfied from the parameter values

2. $a^2 > 0$ this is satisfied due to the positivity of the parameters involved

3. $\frac{D_v}{D_u} > \frac{a^2}{b-1} \implies 80 > 1.038$. We see that this high difusivity ratio means this condition is satisfied

4. $(D_v(b-1) - D_u a^2)^2 > 4D_v D_u a^2 \implies 0.22595 > 0.002$

We see that all 4 of our conditions have been satisfied and this means that we should expect to see patterns from our simulations which is what is backed up by the left image in figure 4.3.
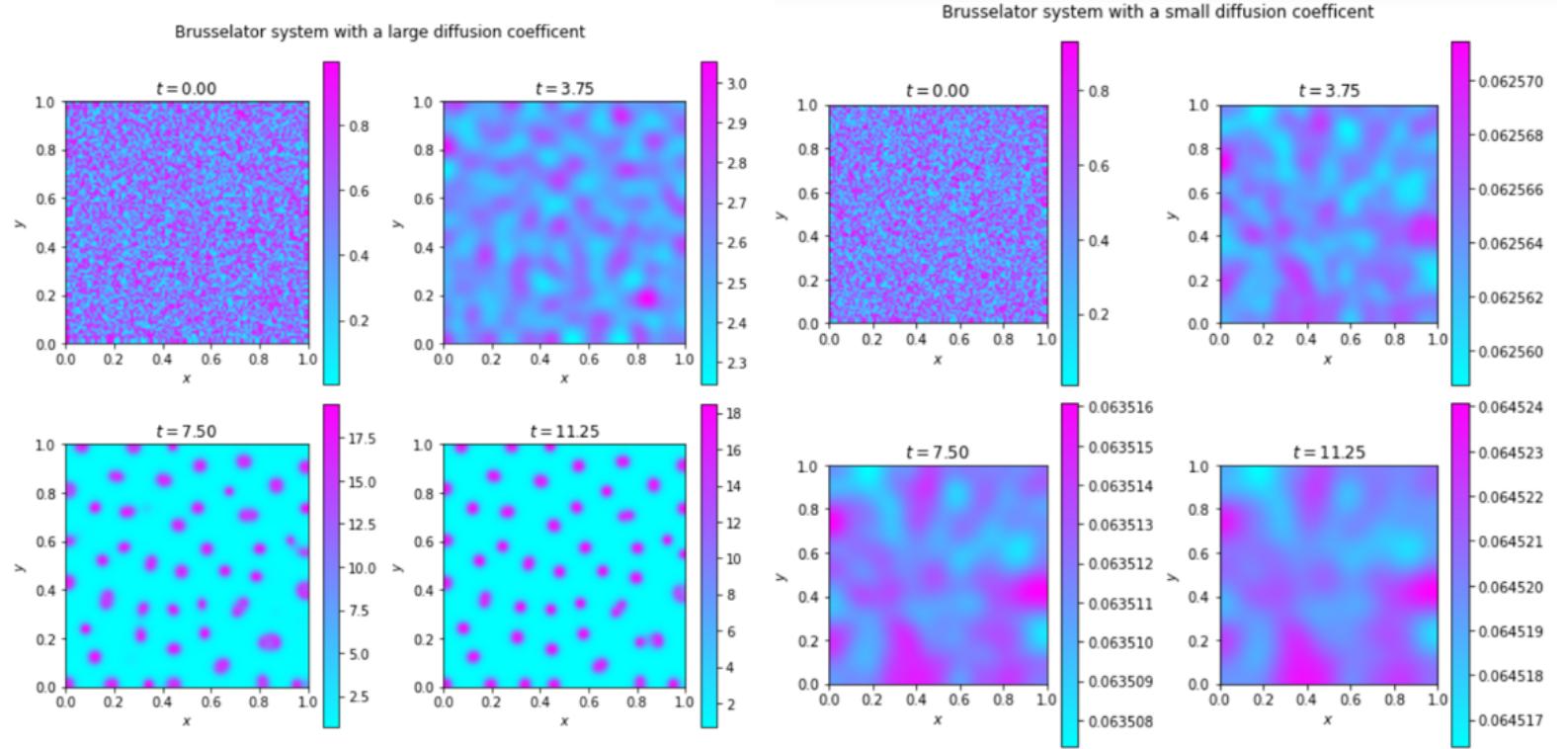
Figure 4.4: System (2.4) for parameter values $a = 2.5, b = 7.02$. The left image $D_u = 0.001, D_v = 0.08$. The right image $D_u = 0.001, D_v = 0.0008$

We can check the critical diffusivity value d_c this was derived in section 3.3.2. Which for our given parameters we get a value of $d_c = 1.2484$. Our simulation on the left we have a diffusion ration of $d = 80 > d_c$ hence why we get such strong spot patterns. When we reduce our diffusion ratio to a value to below this given point, for the simulation on the right we use $d = 0.8 < d_c$ we expect that the system would tend towards a steady homogeneous state which it appears to be doing from the simulation. Hence, we can say for this model our theoretical results match up nicely with our simulations.

4.3.2 Stochastic Simulations

We know the critical Turing bifurcation value for our given parameters is $d_c = 1.2484$. We then choose $D_u = 0.001$ and $D_v = 0.0012484$, choosing these values we gain a diffusion ratio of $d = 1.2484$ which is exactly the critical bifurcation where we would expect patterns to occur for our parameters. Doing this will allow us to investigate the effect of noise on the Brusselator model.
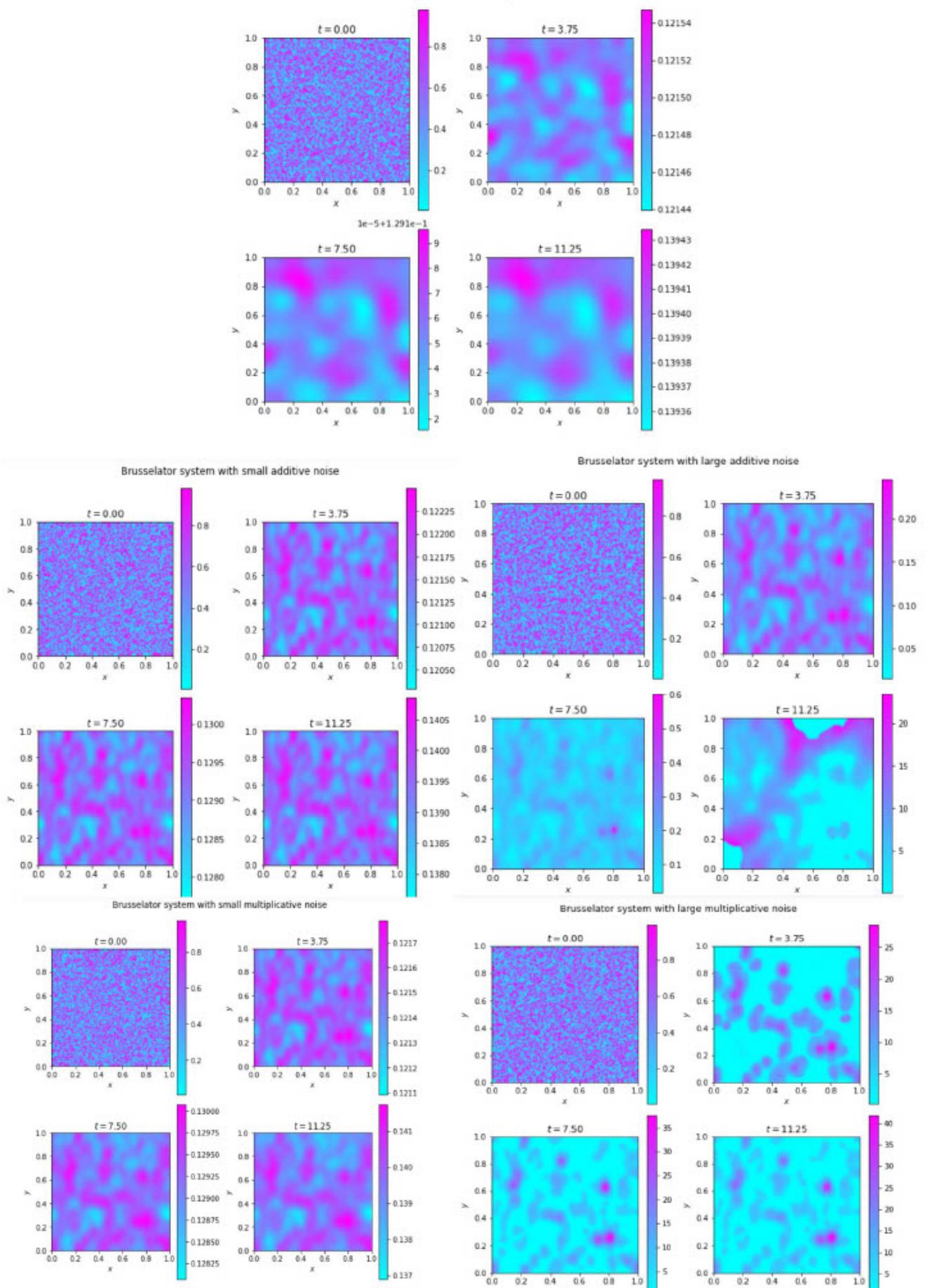
Figure 4.5: System (2.4) for parameter values $a = 2.5, b = 7.02, D_u = 0.001, D_v = 0.0012484$. Top left: $\sigma_1 = \sigma_2 = 0.005$, Top right: $\sigma_1 = \sigma_2 = 0.5$, Bottom left: $\sigma_1 = c_u u, \sigma_2 = c_v v$ where $c_u = c_v = 0.005$, Bottom right: $\sigma_1 = c_u u, \sigma_2 = c_v v$ where $c_u = c_v = 0.5$

Looking at the top simulation which sits on the systems Turing bifurcation. We see very weak indications of spot like patterns as seen in (Figure 4.3) for a large diffusion coefficient. Purple appears to be breaking through the blue periodically, despite it been weak I feel this is a good indication that we are indeed on the Turing bifurcation.

Additive Noise

We will consider the Top left and Top right images of (Figure 4.4) here.

We see that even with a small amount of noise induced, the weak patterns that we had seen are ruined so there is no such patterns at all, it appears as if the additive noise here appears to act as an additional diffusion coefficient for the two chemicals causing them to become more stable and mix well.

Now considering the Top right image. In the FHN model we saw that this larger noise magnitude was able to induce new patterns into the system that we hadn't seen before and we saw higher chemical density's. However, when we use this larger noise magnitude we see a much more random spread of aggregation with no real clear and distinct patterns emerging. We do see however incredibly high concentrated densities of the chemical u-purple. This does imply that at this stage the noise has taken over the system and the chemicals can't interact correctly to form the patterns we expect.

In the SBru model with additive noise, we see that just a small addition of noise into the system knocks the system the wrong way and will not induce patterns into the system. This is an interesting results as for the SFHN the opposite was true. If the noise does get too big eventually the noise will take over and patterns in the system can't emerge.

Multiplicative Noise

Now we analyse the Bottom left and the Bottom right

For low intensity multiplicative noise we see that like in the additive case the weak patterns that were exhibited are destroyed however we do see higher density of the chemical u. However, when we increase the intensity to $c_u = c_v = 0.5$ we see that this intensity just completely destroys the system almost pushing it towards a complete steady state. We see that the high intensity multiplicative noise causes pockets of aggregation of the chemical u where almost all of the chemical is concentrated.

For the SBru model it appears that we can not induce patterns when the intensity of the noise is small or large, and this holds for both when the noise is multiplicative or additive. We see that clearly this system is very sensitive to changes in its spatial dynamics and any extra forcing in the system can lead to its collapse. This is an interesting result as in the FHN model we saw that the additional noise induced different modes and patterns that could not be achieved through deterministic simulations occur. In the Bru model it

appears that when the systems sits on its Turing bifurcation additonal noise knocks the system further away from its critical bifurcation point meaning that patterns can't occur.

4.4 Schnakenberg model

4.4.1 Deterministic Simulations
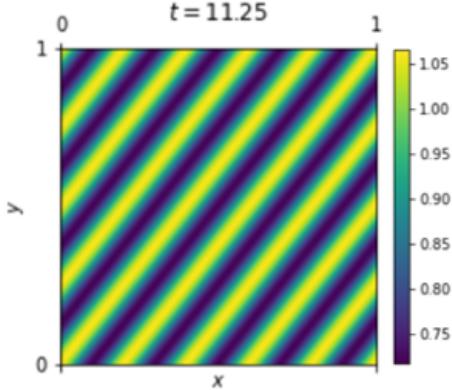
This is potentially one of the most interesting models that will examine we see that the model can exhibit a variety of different patterns for different parameter values. We see that for the same diffusion coefficient we exhibit both spots and stripes this implies that in our simulations different modes are been selected when we change the value of the parameters. Here we shall only look at the end time simulation above in order to concentrate the complex nature of the patterns demonstrated. We shall perform the analysis on stripes however the same can be done with spots also.

Recall we made the transformation of set $b - a = \alpha, a + b = \beta$ hence $\alpha = 0.8, \beta = 1$. The conditions we have to satisfy for pattern formation are as follows
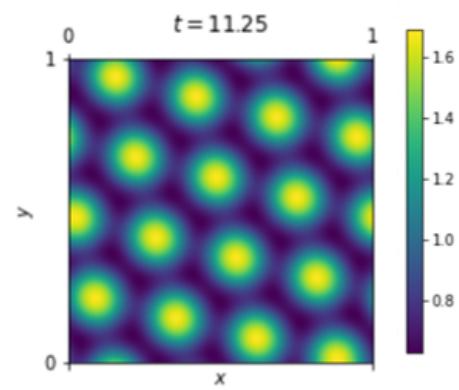
1. $\alpha < \beta^3 \implies 1^3 > 0.8$

2. $\beta^2 > 0$ satisfied as all parameters are greater than 0.

3. $\frac{D_v}{D_u} > \frac{\beta^3}{\alpha} \implies 10 > 1.25$ we see that we require b¿a to ensure a positive diffusion coefficient which is satisfied. But also the conditon enforced by point 3 is satisfied.

4. $(D_v\alpha - D_u\beta^3)^2 > 4D_uD_v\beta^4 \implies 196 > 160$

We see that all 4 of our conditions have been satisfied and this means that we should expect to see patterns from our simulations which is what is backed up by the top left simulation of (Figure 4.5). When we check the conditions for the different parameter values we note that the conditions are also satisfied just we then get spots instead of stripes when simulating.
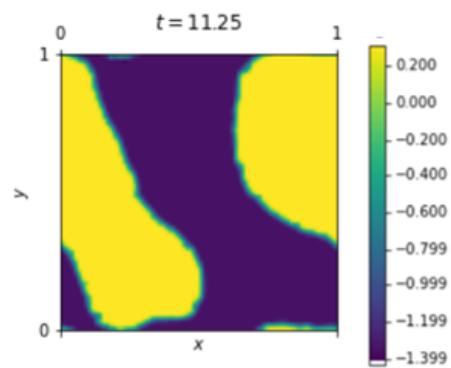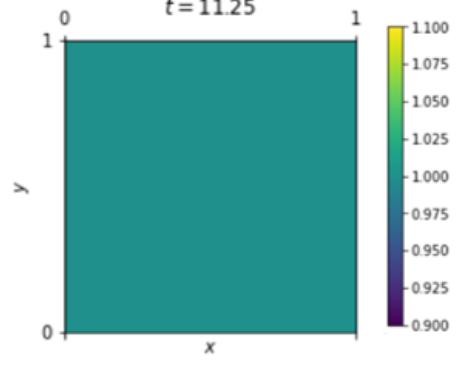
Figure 4.6: System (2.5) for parameter values $D_u = 2, D_v = 10$ for the top row. $D_u = 100, D_v = 10$ for the bottom row. To exhibit stripes we use parameters $a = 0.1, b = 0.9$. For spots we use $a = 0.25, b = 2.25$

We can check the critical diffusivity value d_c this was defined in section 3.3.3. Which for our given parameters we get a value of $d_c = 3.6323$, when we reduce our diffusion ratio to a value to below this given point we expect that patterns do not appear, bottom row of (Figure 4.5) we use $d = 0.1 < d_c$. We see that our theoretical results match up nicely with our simulations.

We see on the bottom row of (Figure 4.5) more than any others what happens when we reduce the diffusion coefficient to a very small value, smaller than the critical diffusion ratio, in one of the simulations we just receive a homogeneous steady state where we would have normally got spots with a normal diffusion parameter. For the situation where we would get stripes we see some slight mixing but nothing that can constitute a pattern.

4.4.2 Stochastic Simulations

As seen before we can get spots or stripes, when we simulate the deterministic model close to the models critical bifurcation point we notice that we get very similar patterns just with different modes for the comparison please see appendix (). Hence we shall proceed with the parameter set that generated stripes in the deterministic case. Note that the critical diffusion point is changed respective to the parameter values changing in the spots case.

We have seen for the SSch $d_c = 3.6323$. We then choose $D_u = 10, D_v = 36.323$ using these values will give us a diffusion ratio of $d = 3.3623$. Which is exactly the critical Turing bifurcation. We can see from the top simulation that when we are sitting exactly on the Turing bifurcation striped patterns do appear however they are not as well defined as in (Figure 4.5).

Additive Noise

Looking at the first row in (Figure 4.6), when we add just a small amount of noise to the system we see that a different mode is induced, it appears as if the system is shifted to presenting spot like patterns of the blue chemical. We have seen this occur previously in other models. However when we add a larger amount of noise to the system that the patterns are completely destroyed and it looks as if the noise has completely taken over in the system.

In the SCK model with additive noise, we notice that a small amounant of additive noise can induce a new mode into the system creating patterns that have not previously been observed however as with most models if the noise intensity becomes too strong the model can can present no patterns at all.
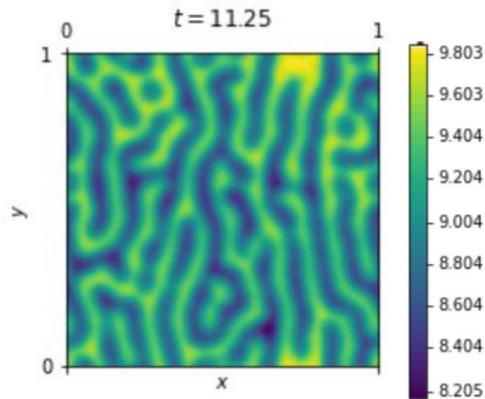
Multiplicative Noise

When we add a weak multiplicative noise to the system we see that in this instance it appears almost like a weaker version of its additive counterpart with the same intensity. This could suggest that the multiplicative noise is too strong for the system even at low intensity values.
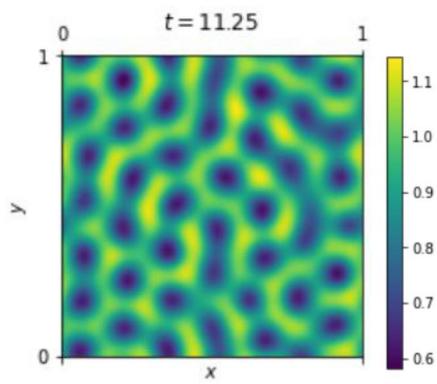
When the intensity of the multiplicative noise is raised to a much larger value we see once again that the noise takes over and the system can't exhibit patterns.

Overall with the SCK model we see that any slight noise that is introduced to system when it is near its critical Turing bifurcation point can induce a new mode creating patterns unseen in the deterministic setting, however we do notice that there is very little difference between the multiplicative and additive noise for this model.
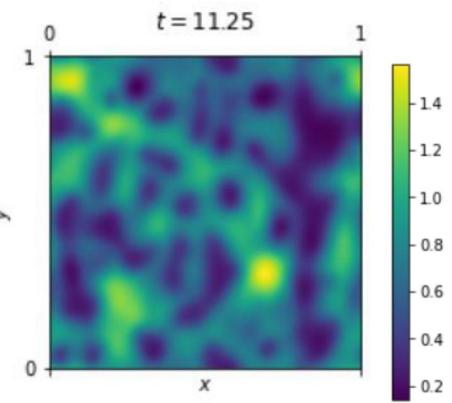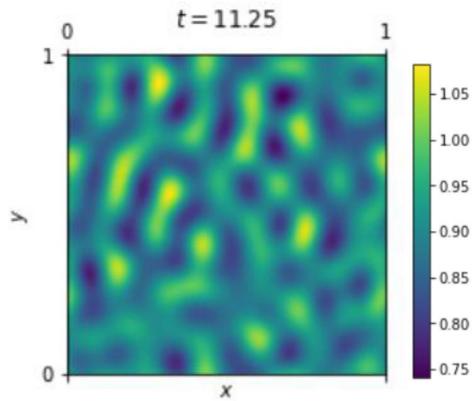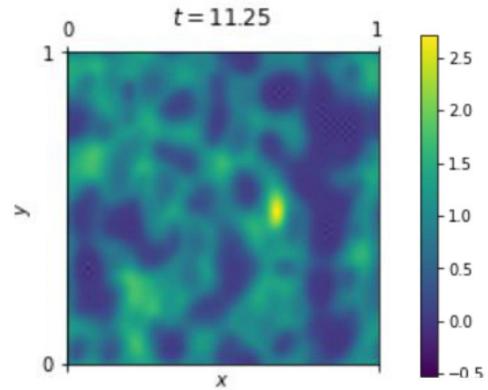
Figure 4.7: System (2.5) for parameter values $a = 0.1, b = 0.9, D_u = 10, D_v = 36.323$. Top left: $\sigma_1 = \sigma_2 = 0.005$, Top right: $\sigma_1 = \sigma_2 = 0.5$, Bottom left: $\sigma_1 = c_u u, \sigma_2 = c_v v$ where $c_u = c_v = 0.005$, Bottom right: $\sigma_1 = c_u u, \sigma_2 = c_v v$ where $c_u = c_v = 0.5$

4.4.3 Comments on the Perturbed system

Considering numerical simulations of systems (2.9,2.10,2.11) would not have enhanced our knowledge of the effect of noise on a system mainly due to the perturbation been deterministic. What we were able to observe in the PFHN was that stronger the perturbation the less clear and distinct the patterns became showing a shift of mode in the systems. When we looked at (2.10) we were able to see that the system could still exhibit rigid pattern formation even when the intensity of the perturbation was large, this could imply that the conditions we derived (3.18) were still satisfied for the PBru models parameters where as the parameters used in the PFHN would not have satisfied (3.18). Another interesting result comes from the PSch, in (A.1.3). We are able to see that when the deterministic perturbation is small we are able to knock the system into a different mode exhibiting new patterns. When the perturbation becomes much larger we see that the system is pushed towards a homogenous steady state which is in line with the theory. When this occurs it can lead us to believe that the conditions derived in (3.18) are not satisfied.

4.5 Numerical simulations of Chemotaxis

4.5.1 Deterministic (Dd)

In this section we shall explore the theoretical results compared to the simulations in a deterministic setting, recall system (2.19)
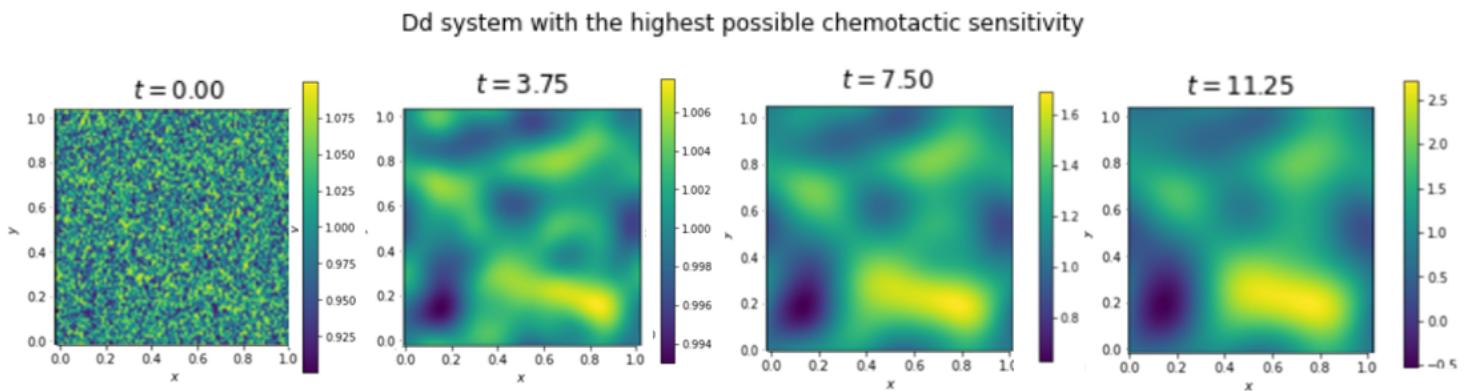

Figure 4.8: A simulation of (2.19) here $D_u = D_v = 10^{-3}, a = b = 1, r = 0.0001, \chi = 1 \cdot 10^{-4}$

Clearly from figure 4.22 we can see that the cells (yellow parts) do begin to move together as more and more waves of cAMP are released. In line with what is expected from this biological problem.

We now compare with the conditions we derived (3.30), now we will plug in the parameter values given

1. $-r - b < 0 \implies -0.0001 - 1 = -1.0001 < 0$ we see that this is satisfied

2. $rb > 0 \implies 0.0001 \cdot 1 = 0.0001 > 0$ we see this condition is also satisfied.

3. $\chi > \frac{1}{a}(rD_v + bD_u) \implies \chi > 1.001 \cdot 10^{-3}$ this provides us a condition for for how big the chemotactic sensitivity has to be.

4. $(\chi a - rd - b)^2 > 4rdb$. We were able to solve for the chemotactic sensitivity to get a new condition for how big χ has to be. $\chi > \frac{D_u}{a}(rd + b + 2\sqrt{rdb})$ where $d = \frac{D_u}{D_v} \implies \chi > 1.0201$.

We then can hence derive that the critical chemotactic sensitivity for which we expect aggregation to occur is at $\chi* = 1.0201$ hence any value greater than this we expect the steady state to become unstable and patterns will begin to appear from this we can conclude $\chi*$ is our chemotactic bifurcation point. We see from our numerical simulations that we do have clear aggregation however we do not have pattern formation this is due to the fact that we are not able to satisfy the

4.5.2   Stochastic Dd

Now we take a look at the Keller Segel model which is then perturbed by time dependent Wiener process (Definition 2.6). Due to computational cost we are only able to simulate the case where we don't consider a spatial element to the noise. We can write the general model in the form

$$
\begin{aligned}
\frac{\partial u}{\partial t} &= D_u \Delta u - \chi \nabla(u\nabla v) + ru(1-u) + \sigma dW(t), \\
\frac{\partial v}{\partial t} &= D_v \Delta v + au - bv + \sigma dW(t)
\end{aligned}
\tag{4.1}
$$

Where $W(t)$ represents the standard Wiener process (Definition 2.4).

Due to us only simulating time dependent Brownian motion we then simulate this through using the Euler-Maruyama method [31] which simulates

$$\sigma dW \sim \sqrt{dt} \cdot \sigma \zeta_n$$

Where $\zeta_n \sim N(0,1)$. See code in (B.4.2) for details.
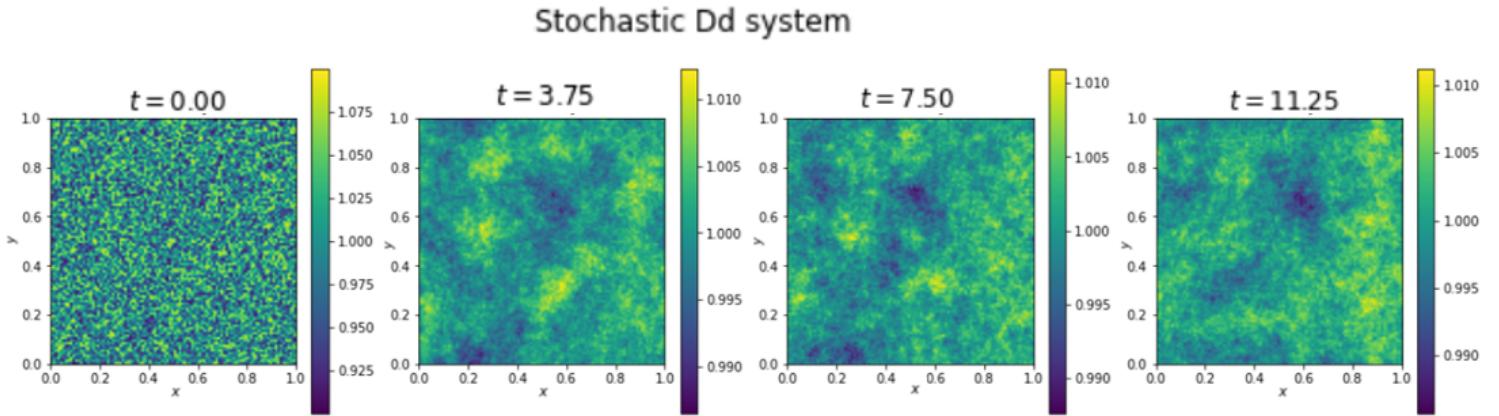
Figure 4.9: A simulation of (2.21) here $D_u = D_v = 10^{-3}, a = b = 1, r = 0.0001, \chi = 1 \cdot 10^{-4}$ with spatial homogenous white noise

For this chemotactic simulation we use $\chi = 10^{-4}$ which is the highest available to us computationally. We see clearly that there is no clear indications that patterns will occur at all. This simulation has been averaged over many realisations.

In conclusion we can see that when a stochastic forcing is applied to the model unlike the reaction diffusion setting where we could play around the bifurcation point to see how forcing could affect patterns in the chemotaxis setting we see that the stochastic forcing takes over the model with no indication of pattern formation at all.

4.5.3   Comments on PDd

We see when we added the deterministic perturbation to the system that the results follow in line with what we would expect that the stronger the perturbation the less aggregation we see in the model. See A.1.4

Appendix A

Perturbed Numerical Simulations

A.1   Biological Systems

For all of our systems the perturbation requires a variance to be given, following [**29**] we use $\sigma = 0.5$.

A.1.1 PFHN
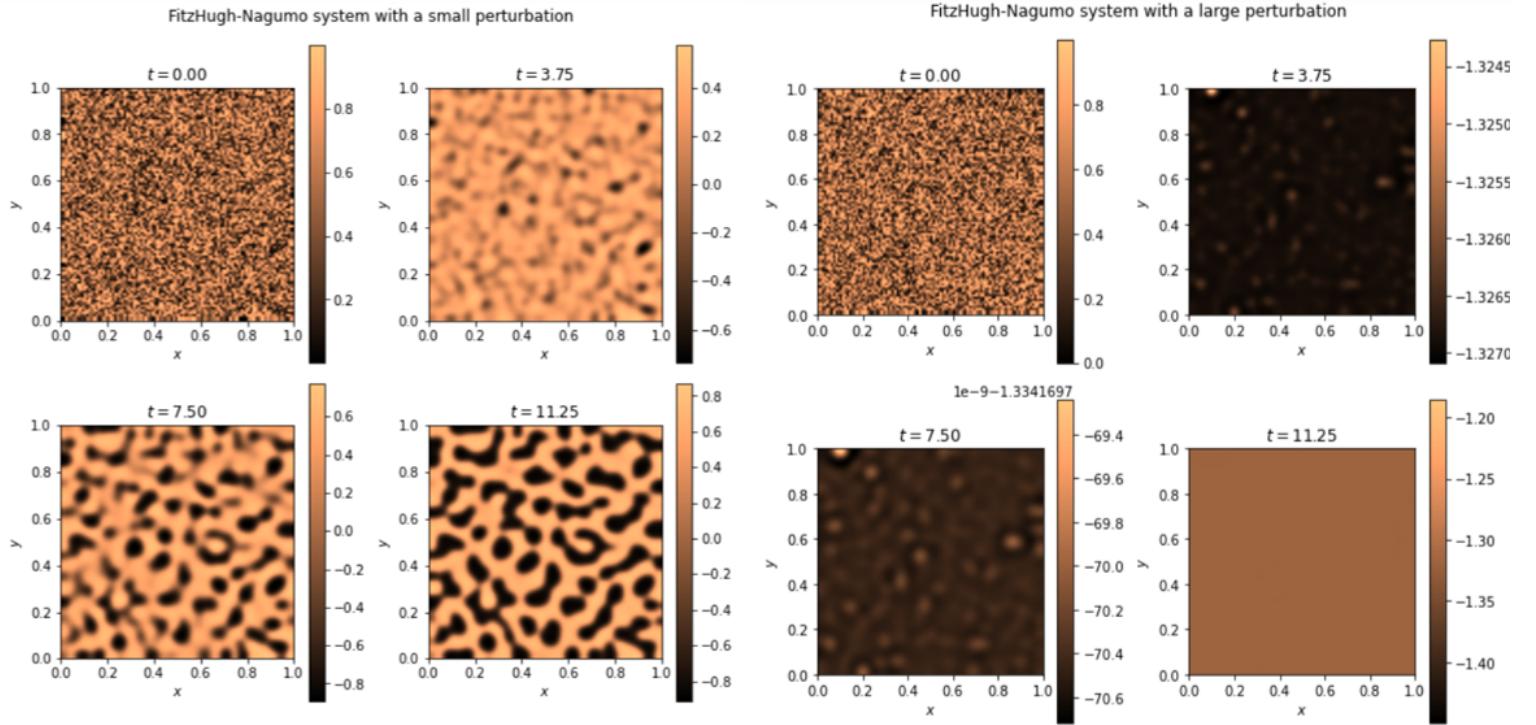
Figure A.1: System (2.3) for parameter values $a = 3.42, b = 1.21, e = 1, D_u = 2.8 \cdot 10^{-4}, D_v = 5.3 \cdot 10^{-3}$. The left image $D_1 = 1 \cdot 10^{-5}, D_2 = 1 \cdot 10^{-5}$. The right image $D_1 = 1 \cdot 10^{-1}, D_2 = 1 \cdot 10^{-1}$

A.1.2   PBru
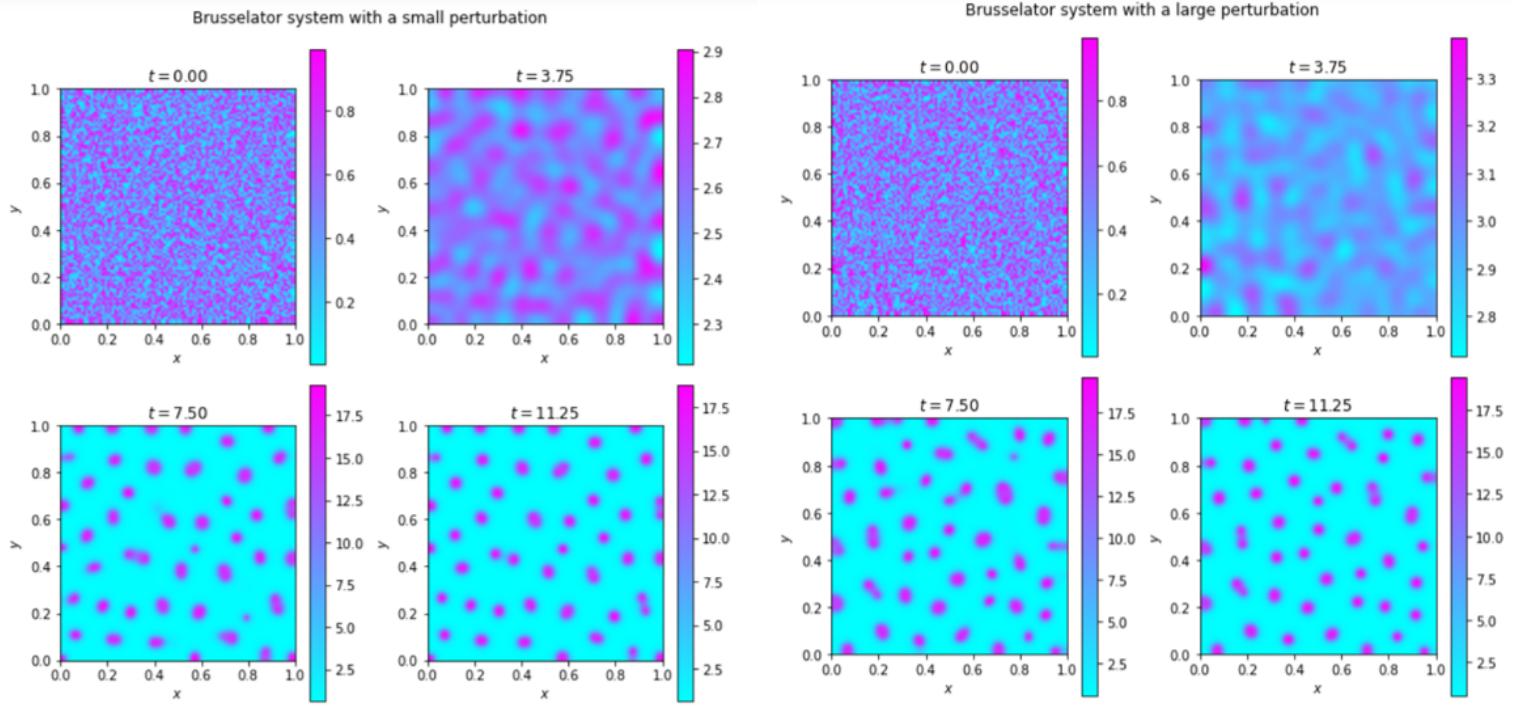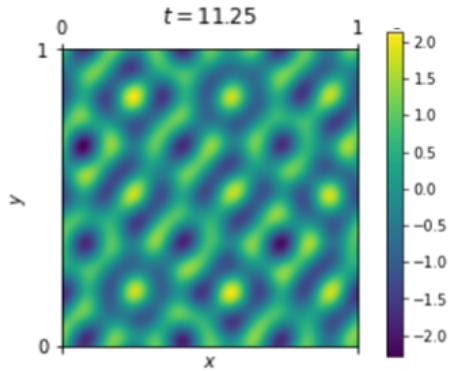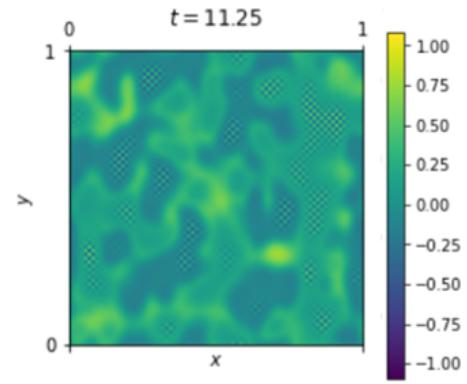
Figure A.2: System (2.4) for parameter values $a = 2.5, b = 7.02, D_u = 0.001, D_v = 0.08$. The left image $D_1 = 1 \cdot 10^{-5}, D_2 = 1 \cdot 10^{-5}$. The right image $D_1 = 1 \cdot 10^{-1}, D_2 = 1 \cdot 10^{-1}$

A.1.3 PSch
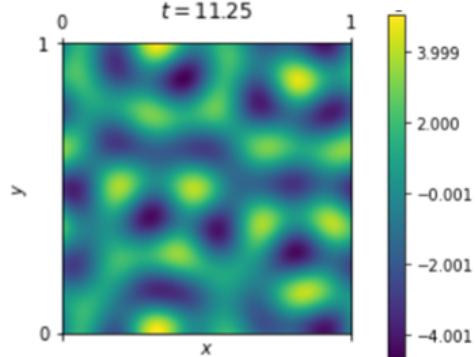
Figure A.3: System (2.5) for parameter values $D_u = 2, D_v = 10$ for all simulations. To exhibit stripes we use parameters $a = 0.1, b = 0.9$. For spots we use $a = 0.25, b = 2.25$ Here on the left $D_2 = D_4 = 10^{-5}$ and on the right $D_2 = D_4 = 10^{-1}$

A.1.4   Sch close to Turing bifurcation

Schnakenberg system exhibiting stripes, on the Turing Bifurcation

Schnakenberg system exhibiting spots, on the Turing Bifurcation
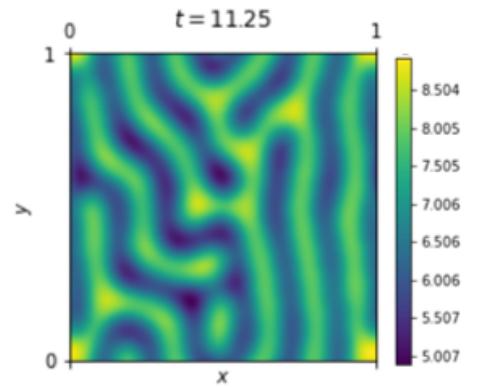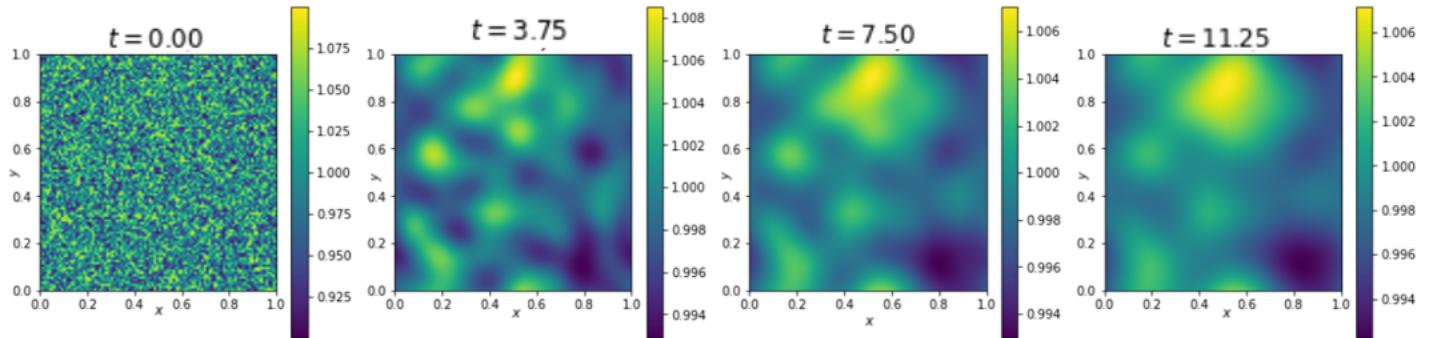
Figure A.4: System (2.5) for parameter values $D_u = 10, D_v = 36.323, a = 0.1, b = 0.9$ for the left image. $D_u = 10, D_v = 15.2, a = 0.25, b = 2.25$ for the right image.

A.1.5   PDd
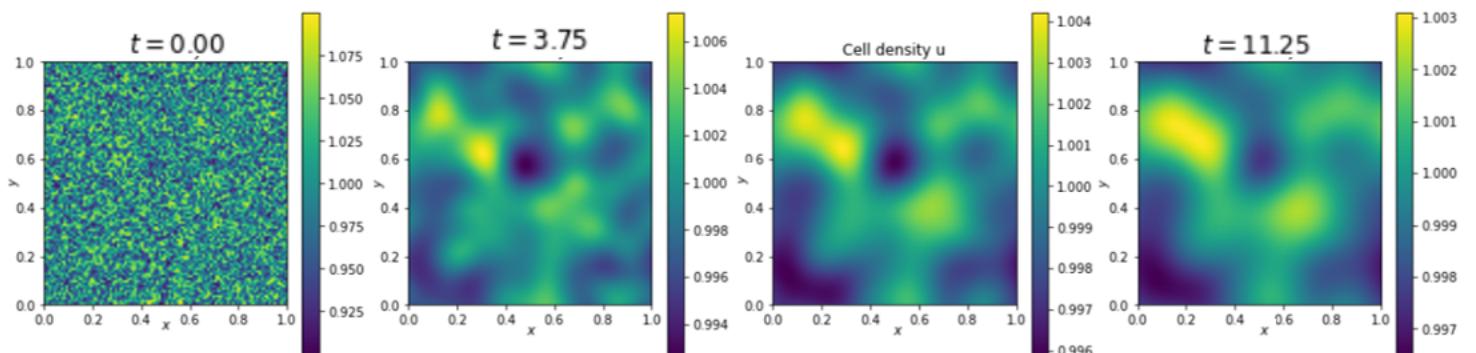
Figure A.5: A simulation of (2.20) here $D_u = D_v = 10^{-3}, a = b = 1, r = 0.0001, \chi = 1 \cdot 10^{-4}$. Here at the top $D_1 = D_2 = 10^{-5}$ then on the bottom row $D_1 = D_2 = 10^{-1}$

Appendix B

Code For Simulations

We shall provide the basic out line for the code for which it can be changed to suit each individual model.

B.1 Deterministic simulations

```
import numpy as np
import matplotlib.pyplot as plt


#constants
a=2.5
difu=0.001
difv=0.08 # difu=0.0008 for smaller diffusion coefficient
b=7.02
#Change the parameters accordingly for FHN & Sch

s = 100  # 2D grid size
dx = 2.0/s  # spatial step

T = 15  # end time
dt = 0.001  # time step
n = int(T /dt)  # num of iterations

U = np.array(np.random.rand(s, s))
#using random noise from 0 to 1 as initial cond
V = np.array(np.random.rand(s, s))

def Lap(L):
    Ltop = L[0:−2, 1:−1]
```

```
    Lleft = L[1:-1, 0:-2]
    Lbottom = L[2:, 1:-1]
    Lright = L[1:-1, 2:]
    Lcenter = L[1:-1, 1:-1]
    return (Ltop + Lleft + Lbottom + Lright -
        4 * Lcenter) / dx**2


def show_pat(U, ax=None):
    ax.imshow(U, cmap=plt.cm.cool,
        interpolation='bilinear',
        extent=[0, 1, 0, 1])
    ax.set_axis_on()
    ax.set_xlabel(r'$x$')
    ax.set_ylabel(r'$y$')



fig, axes = plt.subplots(2, 2, figsize=(8, 8))
step_plt = n // 4
# using the finite difference method
for i in range(n):
# We compute the Laplacian of u and v.
    deltaU = Lap(U)
    deltaV = Lap(V)


# We take the values of u and v inside the grid.
    Uc = U[1:-1, 1:-1]
    Vc = V[1:-1, 1:-1]


# We update the variables through finite difference
    U[1:-1, 1:-1], V[1:-1, 1:-1] = \
        Uc + dt * (f(u,v)), \
        Vc + dt * (g(u,v))
        # Here inside the bracket this where you put the
        #different kinetic functions
        # e.g for Bru model f(u,v)=difu * deltaU + a-(b+1)*Uc+Uc**2*Vc
         # g(u,v)= b * Uc-Uc**2*Vc+difv*deltaV
# Imploring Neumann conditions derivatives at the edges are zero.
    for L in (U, V):
        L[0, :] = L[1, :]
        L[-1, :] = L[-2, :]
        L[:, 0] = L[:, 1]
        L[:, -1] = L[:, -2]
```

```
# Plotting of the system
    if i % step_plt == 0 and i < 4 * step_plt:
        ax = axes.flat[i // step_plt]
        show_pat(U, ax=ax)
        ax.set_title(f'$t={i * dt:.2f}$')
        p=ax.imshow(U, cmap=plt.cm.cool,
        interpolation='bilinear',
        extent=[0, 1, 0, 1])
        fig.colorbar(p,ax=ax)
        fig.tight_layout(rect=[0, 0.03, 1, 0.95])
        fig.suptitle('Brusselator system with a large diffusion coefficent')
```

B.2   Perturbed Simulation

```
import numpy as np
import matplotlib.pyplot as plt


#constants
a=2.5
difu=0.001
difv=0.08 # difu=0.0008 for smaller diffusion coefficient
D_1 = 10**-5 #D_1 = 10**-1
D_2 = 10**-5 #D_2 = 10**-1 for large perturbation
b=7.02
#Change the parameters accordingly for FHN & Sch
uS = a
vS = a/b
# These are the steady states for the Bru model,
# change accordingly for FHN and Sch

s = 100  # 2D grid size
dx = 2.0/s  # spatial step

T = 15  # end time
dt = 0.001  # time step
n = int(T /dt)  # num of iterations

U = np.array(np.random.rand(s, s))
#using random noise from 0 to 1 as initial cond
V = np.array(np.random.rand(s, s))
```

```python
def Lap(L):
    Ltop = L[0:-2, 1:-1]
    Lleft = L[1:-1, 0:-2]
    Lbottom = L[2:, 1:-1]
    Lright = L[1:-1, 2:]
    Lcenter = L[1:-1, 1:-1]
    return (Ltop + Lleft + Lbottom + Lright -
        4 * Lcenter) / dx**2

def show_pat(U, ax=None):
    ax.imshow(U, cmap=plt.cm.cool,
        interpolation='bilinear',
        extent=[0, 1, 0, 1])
    ax.set_axis_on()
    ax.set_xlabel(r'$x$')
    ax.set_ylabel(r'$y$')


fig, axes = plt.subplots(2, 2, figsize=(8, 8))
step_plt = n // 4
# using the finite difference method
for i in range(n):
# We compute the Laplacian of u and v.
    deltaU = Lap(U)
    deltaV = Lap(V)

# We take the values of u and v inside the grid.
    Uc = U[1:-1, 1:-1]
    Vc = V[1:-1, 1:-1]

# We update the variables through finite difference
    U[1:-1, 1:-1], V[1:-1, 1:-1] = \
        Uc + dt * (f(u,v) + (D_1*Uc-D_1*uS)*np.random.normal(a,0.5)), \
        Vc + dt * (g(u,v) + (D_2*Vc-D_1*vS)*np.random.normal(a/b,0.5)) )
        # Here inside the bracket this where you put the
        #different kinetic functions
        # e.g for Bru model f(u,v)=difu * deltaU + a-(b+1)*Uc+Uc**2*Vc
         # g(u,v)= b * Uc-Uc**2*Vc+difv*deltaV
        # Adding the deterministic perturbation on the
        #end around the respective steady states for U and V
# Imploring Neumann conditions derivatives at the edges are zero.
    for L in (U, V):
```

65

```
        L[ 0 ,  : ]  = L[ 1 ,  : ]
        L[−1,  : ]  = L[−2,  : ]
        L [ : ,  0] = L [ : ,  1]
        L [ : ,  −1] = L [ : ,  −2]

# Plotting  of  the  system
    if  i % step_plt == 0  and  i < 4 * step_plt :
        ax = axes . flat [ i // step_plt ]
        show_pat (U,  ax=ax )
        ax . set_title ( f ' $t={i * dt :.2 f }$ ')
        p=ax . imshow (U,  cmap=plt .cm. cool ,
        interpolation =' bilinear ',
        extent =[0 ,  1 ,  0 ,  1])
        fig . colorbar (p , ax=ax )
        fig . tight_layout ( rect =[0 ,  0.03 ,  1 ,  0.95])
        fig . suptitle ( ' Brusselator  system  with  a  small  perturbation ')
```

B.3   Stochastic simulation

B.3.1   Q-Wiener process

```
from  math  import *
# Numpy
import  numpy  as  np
from  numpy  import  matlib
fft=np . fft . fft
fft2=np . fft . fft2
ifft=np . fft . ifft
ifft2=np . fft . ifft2
# Plotting
%matplotlib  inline
import  matplotlib
import  matplotlib . pyplot  as  plt
from  mpl_toolkits . mplot3d  import  Axes3D
from  matplotlib  import  cm
# Scipy
import  scipy
from  scipy  import  sparse
from  scipy . sparse  import  linalg
from  scipy  import  optimize
from  scipy  import  fftpack
#
```

```
def icspde_dst1(u):
    return scipy.fftpack.dst(u,type=1,axis=0)/2


fft2=np.fft.fft2
ifft2=np.fft.ifft2
#
def get_twod_bj(dtref,J,a,alpha):
    """
    Alg 4.5 Page 443
    """
    lambdax=2 * pi * np.hstack([np.arange(0,J[0]//2 +1),
    np.arange(- J[0]//2 + 1,0)]) / a[0]
    lambday=2 * pi * np.hstack([np.arange(0,J[1]//2 +1),
    np.arange(- J[1]//2 + 1,0)]) / a[1]
    lambdaxx,lambdayy=np.meshgrid(lambdax,lambday,indexing='ij')
    root_qj=np.exp(- alpha * (lambdaxx ** 2 + lambdayy ** 2) / 2)
    bj=root_qj * sqrt(dtref) * J[0] * J[1] / sqrt(a[0] * a[1])
    return bj
#
def get_twod_dW(bj,kappa,M):
    """
    Alg 10.6 Page 444
    """
    J=bj.shape
    if (kappa == 1):
        nn=np.random.randn(M,J[0],J[1],2)
    else:
        nn=np.sum(np.random.randn(kappa,M,J[0],J[1],2),0)
    nn2=np.dot(nn,np.array([1,1j]));
    tmp=ifft2(bj*nn2)
    dW1=np.real(tmp)
    dW2=np.imag(tmp)
    return dW1,dW2
```

B.3.2   Stochastic simulation

```
import numpy as np
import matplotlib.pyplot as plt



#constantes
a=2.5
```

```
difx=0.001
dify=0.0012484
sig_1=0.005
sig_2=0.005 # sig=0.5 for larger noise
b=7.02
# Change for FHN and Sch

s = 100  # size of the 2D grid
dx = 2.0 / size   spatial step

T = 15  # total time
dt = 0.001  # time step
n = int(T / dt)  # num of iterations

U = np.array(np.random.rand(size, size))  #
#random noise from 0 to 1.
V = np.array(np.random.rand(size, size))

def Lap(L):
        Ltop = L[0:-2, 1:-1]
        Lleft = L[1:-1, 0:-2]
        Lbottom = L[2:, 1:-1]
        Lright = L[1:-1, 2:]
        Lcenter = L[1:-1, 1:-1]
        return (Ltop + Lleft + Lbottom + Lright -
                4 * Lcenter) / dx**2

def show_pat(U, ax=None):
        ax.imshow(U, cmap=plt.cm.cool,
                interpolation='bilinear',
                extent=[-1, 1, -1, 1])
        ax.set_axis_on()
        ax.set_xlabel(r'$x$')
        ax.set_ylabel(r'$y$')

fig, axes = plt.subplots(2, 2, figsize=(8, 8))
step_plot = n // 4
# Finite difference
for j in range(100):
    J=[98,98]; dtref=0.01; kappa=100; a=[2*pi,3*pi]
    alpha=0.05; bj=get_twod_bj(dtref,J,a,alpha)
    W1,W2=get_twod_dW(bj,kappa,1)
    for i in range(n):
```

```
# We compute the Lap of u and v.
    deltaU = Lap(U)
    deltaV = Lap(V)
# We take the values of u and v inside the grid.
    Uc = U[1:-1, 1:-1]
    Vc = V[1:-1, 1:-1]

#We update the variables.
    U[1:-1, 1:-1], V[1:-1, 1:-1] = \
            Uc + dt * (f(u,v) + sig_1*W1[0,:,:]), \
            Vc + dt * (g(u,v) sig_1*W1[0,:,:])
# Swap out for the specific model equations
    # add *Vc next to W1 to make the noise multiplicative

    for L in (U, V):
            L[0, :] = L[1, :]
            L[-1, :] = L[-2, :]
            L[:, 0] = L[:, 1]
            L[:, -1] = L[:, -2]

# plotting
    if i % step_plt == 0 and i < 4 * step_plt:
        ax = axes.flat[i // step_plot]
        show_plt(np.mean(U), ax=ax)
        ax.set_title(f'$t={i * dt:.2f}$')
        p=ax.imshow(U, cmap=plt.cm.cool,
        interpolation='bilinear',
        extent=[0, 1, 0, 1])
        fig.colorbar(p,ax=ax)
        fig.tight_layout(rect=[0, 0.03, 1, 0.95])
        fig.suptitle('Brusselator system with small additive noise')
```

B.4   Chemotaxis

B.4.1   Deterministic

```
import numpy as np
import matplotlib.pyplot as plt
%matplotlib inline

s = 100 # size of grid
ds = 1. / n # spatial resolution, assuming space is [0,1] * [0,1]
```

```python
dt = 0.01 # temporal resolution


Du = 10**-3 # diffusion constant of u
Dv = 10**-3 # diffusion constant of v
r = 0.0001
a = 1. # production of cAMP by Dictyostelium cells.
b = 1.  # degradation of cAMP by proteolytic enzymes.
chi = 1.*10**-4 #chemotactic sensitivty

v = np.zeros([s, s])
u = np.zeros([s, s])
for x in range(s):
    for y in range(s):
        v[x, y] = 1. + np.random.uniform(-0.1, 0.1) # small noise is added
        u[x, y] = 1. + np.random.uniform(-0.1, 0.1) # small noise is added

nextv = np.zeros([s, s])
nextu = np.zeros([s, s])


def run():
    global v, u, nextv, nextu
    for y in range(s):
        for x in range(s):
            vC, vR, vL, vU, vD = v[y,x], v[(y+1)%s,x], v[(y-1)%s,x],
            v[y,(x+1)%s], v[y,(x-1)%s]
            uC, uR, uL, uU, uD = u[y,x], u[(y+1)%s,x], u[(y-1)%s,x],
            u[y,(x+1)%s], u[y,(x-1)%s]
            # L
            uLap = (uR + uL + uU + uD - 4 * uC) / (ds**2)
            vLap = (vR + vL + vU + vD - 4 * vC) / (ds**2)


            # state-transition function
            A = (Du * uLap)
            B = - chi * ((uR-uL)*(vR-vL)+(uU-uD)*(vU-vD)+4*uC*vLap) +
            r*uC-r*uC**2
            nextu[y, x] = uC + (B+ A) * dt
            nextv[y, x] = vC + (a * uC - b * vC + Dv * vLap ) * dt
    u, nextu = nextu, u
    v, nextv = nextv, v
```

```
plt.figure(figsize=(20,5))

d = 1
for i in range(0, 1251):
    run()
    if i%250 == 0:
        plt.subplot(1,4,d)
        # draw only money, people look the same
        plt.imshow(nextu,interpolation='bilinear', extent=[0, 1, 0, 1])
        x=plt.imshow(nextu,interpolation='bilinear', extent=[0, 1, 0, 1])
        plt.xticks([0,0.2,0.4,0.6,0.8,1]); plt.yticks([0,0.2,0.4,0.6,0.8,1]);
        plt.title('Cell density u')
        plt.colorbar(x)
        d += 1
```

B.4.2   Stochastic

```
import numpy as np
import matplotlib.pyplot as plt
%matplotlib inline

s = 100 # size of grid
ds = 1. / n # spatial resolution, assuming space is [0,1] * [0,1]
dt = 0.01 # temporal resolution

Du = 10**-3 # diffusion constant of u
Dv = 10**-3 # diffusion constant of v
r = 0.0001
a = 1. # production of cAMP by Dictyostelium cells.
b = 1.  # degradation of cAMP by proteolytic enzymes.
chi = 1.*10**-4 #chemotactic sensitivty

v = np.zeros([s, s])
u = np.zeros([s, s])
for x in range(s):
    for y in range(s):
        v[x, y] = 1. + np.random.uniform(-0.1, 0.1) # small noise is added
        u[x, y] = 1. + np.random.uniform(-0.1, 0.1) # small noise is added

nextv = np.zeros([s, s])
nextu = np.zeros([s, s])
```

```
def run():
    global v, u, nextv, nextu
    for y in range(s):
        for x in range(s):
            vC, vR, vL, vU, vD = v[y,x], v[(y+1)%s,x], v[(y-1)%s,x],
            v[y,(x+1)%s], v[y,(x-1)%s]
            uC, uR, uL, uU, uD = u[y,x], u[(y+1)%s,x], u[(y-1)%s,x],
            u[y,(x+1)%s], u[y,(x-1)%s]
            # L
            uLap = (uR + uL + uU + uD - 4 * uC) / (ds**2)
            vLap = (vR + vL + vU + vD - 4 * vC) / (ds**2)


            # state-transition function
            A = (Du * uLap)
            B = - chi * ((uR-uL)*(vR-vL)+(uU-uD)*(vU-vD)+4*uC*vLap)
            + r*uC-r*uC**2
            nextu[y, x] = uC + (B+ A) * dt +
            np.sqrt(dt)*np.random.normal(0,1)
            nextv[y, x] = vC + (a * uC - b * vC + Dv * vLap ) * dt +
            np.sqrt(dt)*np.random.normal(0,1)
            # Simulate Wiener process using Euler method
    u, nextu = nextu, u
    v, nextv = nextv, v


plt.figure(figsize=(20,5))

d = 1
for i in range(0, 1251):
    run()
    if i%250 == 0:
        plt.subplot(1,4,d)
        # draw only money, people look the same
        plt.imshow(nextu,interpolation='bilinear', extent=[0, 1, 0, 1])
        x=plt.imshow(nextu,interpolation='bilinear', extent=[0, 1, 0, 1])
        plt.xticks([0,0.2,0.4,0.6,0.8,1]); plt.yticks([0,0.2,0.4,0.6,0.8,1]);
        plt.title('Cell density u')
        plt.colorbar(x)
        d += 1
```

Appendix C

Well Posedness

C.1   Deterministic

We can say that a problem is well-posed "in the sense of Hadamard" if the following are satisfied

- Existence and uniqueness (C1)

- Existence for all times (C2)

- Continuous dependency on the initial conditions (C3)

However these conditions alone are not sufficient for the biological and physical models that we shall examine as we are working with physical parameters, this means that we can not allow the solution to become negative also the solution must be bounded hence we add two new conditions in order so we can class our problem as well-posed.

- Solution is non-negative for non-negative initial data (C4)

- Solution is bounded for all bounded initial data (C5)

We can apply theory of semigroups and functional analysis to show well-posedness (C1-C5) for the general system (2.1-2.3). Note that the theory of semigroups is set out in Appendix A and important results shall be noted throughout for the reader to visit.

C.1.1   Uniqueness and Local Existence

We state some basic hypotheses which are assumed to hold

- $D_1, D_2 > 0$ (H1)

- $u_0, v_0 \geq 0$ are continuous on $\bar{\Omega}$; $u_0, v_0 \in C^0_{L^\infty}(\Omega)$ (H2)

- f, g are continuously differentiable functions from $\bar{\mathbb{R}}_+^3$ into $\mathbb{R}$ with $f(t, 0, s) \geq 0$ and $g(t, r, 0) \geq 0$ for all $t, r, s \geq 0$ (H3)

- There exist $m > 0$ and a continuous fucntion $F : \bar{\mathbb{R}}_+^2 \implies \mathbb{R}_+$ such that $f(t, r, s), g(t, r, s) \leq exp(mt)F(r, s), \forall t, r, s \geq 0$ (H4)

Note compared to one of the books we are following by [37] we have added (H4) to achieve local existence for $(u_0, v_0) \in (C_{L^\infty}^0)^2$.

Proposition C.1.1 (Local existence see [38] Thm 3.3.1). Given Hypotheses (H1-H4) are satisfied then there exist $T = T(u_0, v_0) > 0$ such that reaction diffusion system (2.1-2.3) has a unique solution $(u, v) \in (C_{L^\infty}^0((0, T]; D(\mathcal{H}^\alpha)))^2$ with $u(0) = u_0 \in C_{L^\infty}^0$ and $v(0) = v_0 \in C_{L^\infty}^0$

C.1.2 Global existence and boundedness

In this section we present the main result of [37] to give sufficient conditions for the system to be global and bounded.
The main Thereom if this section we shall state now:

Theorem C.1.2. Suppose in addition to (H1-H4) the following hypotheses hold:

- N_2 in Proposition 2.1.4 is bounded if $T^* < \infty$ (H5)

- There exists an $\eta > 1$ and a continuous function $h : [0, \infty)^2 \implies [0, \infty)$ such that $|f(t, r, s)| \leq h(t, S)(1 + r)^\eta \forall t, r, s \geq 0$ with $s \leq S$ (H6)

- There exist am $\epsilon > 0$ and a continuous function $l : [0, \infty)^2 \implies [0, \infty)$ such that $\epsilon r + f(t, r, s) + g(t, r, s) \leq l(t, S) \forall t, r, s \geq 0$ with $s \leq S$.

Then the solution exists on $D \times (0, \infty)$ and (2.9), which I will repeat below:

$$0 \leq u \leq N_1(t), 0 \leq v \leq N_2(t) \text{ holds in } D \times [0, T^*)$$

This result holds with $T^* = \infty$.
Moreover, if N_2, h and p are bounded in t,

$$N_2(t) \leq \bar{N}_2, h(t, S) \leq \bar{h}(S), p(t, S) \leq \bar{p}(S) \forall t \geq 0$$

then there exist $\bar{N}_1$ such that $N_1(t) \leq \bar{N}_1, \forall t \in [0, \infty)$ and so the solution is uniformly bounded in $D \times [0, \infty)$

C.2 Stochastic

From the work of [**39**] we state the main results

- f(r,v,x,t) and $\sigma(r, x, t)$ are predictible random fields. We then say there exists a constant $K_1 > 0$ such that

$$||f(u, v, \cdot, t)||^2 + ||\sigma(u, \cdot, t)||^2 \leq K_1(1 + ||u||^2)$$

  for any $u \in L^2, t \in [0, T]$ (C1).

- There exist a constant $K_2 > 0$ such that

$$||f(u, v, \cdot, t) - f(u_1, v, \cdot, t)||^2 + ||\sigma(u, \cdot, t) - \sigma(u_1, \cdot, t)||^2 \leq K_2||u - u_1||^2$$

  for any $u, u_1 \in L^2, t \in [0, T]$ (C2)

- We say that $W(x, t)$ is a Q-Weiner field of finite trace and the covariance function $r(x, y)$ is bounded by r_0, for $x, y \in D$ (C3)

Then one large theorem is

Theorem C.2.1. Let the conditions (C1-C3) be satisfied and let h be a $\mathbb{F}_0-$measurable random field such that $E[||h||^{2p}] < \infty$ for $p \geq 1$. Then the reaction diffusion equation 2.39 has a unique mild solution $u(\cdot, t)$ which is a continous adapted processes in L^2 such that $u \in L^{2p}(\Omega; C([0, T]; L^2))$ satisfying

$$E[\sup_{0 \leq t \leq T} ||u(\cdot, t)||^{2p}] \leq C[1 + E[||h||^{2p}]] \tag{C.1}$$

We have the constant $C > 0$ depending on p, r_0, T. Also, we see that the energy inequality holds

$$E[||u(\cdot, t)||^2] \leq E[||h||^2 + 2\int_0^t (u_s, F_s(u))ds + \int_0^t Tr(Q_s(u))ds] \tag{C.2}$$

Where $Tr(Q_s(u)) = ||\sum_s(u)||_R^2$, this holds for $t \in [0, T]$

Proof. For the proof see [**39**] pg 69 ■

In Therorem 2.2.3 the global conditions on Lipschitz-continuity and C1, C2 on linear growth can be relaxed to hold locally. However if we don't add an additioncal contraint they may lead to a explosive solution in finite time. The additional constraint is

- $f(r, x, t), \sigma(r, x, t)$ are predictable random fields. Then there exists a constant $C_n > 0$ such that

$$||f(u, v, \cdot, t)||^2 + ||\sigma(u, \cdot, t)||^2 \leq C_n$$

  for any $u \in L^2, n > 0$ with $||u|| \leq n, t \in [0, T]$ (C_n.1)

- There exists a constant $K_n > 0$ such that

$$||f(u, v, \cdot, t) - f(u_1, v_1, \cdot, t)||^2 + ||\sigma(u, \cdot, t) - \sigma(u_1, \cdot, t)||^2 \leq K_n ||u - u_1||^2$$

for any $t \in [0, T], u, u_1 \in L^2$ with $||u|| \times ||v|| \leq n$ $(C_n.2)$

- There exist constant $C_1 > 0$ such that

$$(u, f(u, v, \cdot, t)) + 1/2 Tr(Q_t(u) \leq C_1(1 + ||u||^2)$$

for any $u \in L^2, t \in [0, T]$ (A.4)

If the problem has the conditions $C_n.1, C_n.2, C3, C4$ holds the the solutions exists in any finite time interval. The proof is based on a truncation technique by making use of a Mollifier ζ_n on $[0, \infty)$ to be defined now.

Definition C.3 (Mollifier). For $n > 0$, $\zeta_n : [0, \infty) \implies [0, 1]$ is a C^∞-function such that

$$\zeta_n(r) = \left\{ \begin{array}{cc} 1 & 0 \leq r \leq n \\ 0 & r > 2n \end{array} \right. \tag{C.3}$$

Theorem C.3.1 (Local & Global existence). Let the conditions $C_n.1, C_n.2, C3$ be satisfied and let h be a $\mathbb{F}_0$-measurable random field such that $E[||h||^2] < \infty$. Then the reaction diffusion equation (2.39) has a unique local solution $u(\cdot, t)$ which is an adapted, continuous process in L^2. Also if condition $C4$ holds then the solution exists for $t \in [0, T]$ with any $T > 0$ and $u \in L^2(D; C([0, T]; H))$ satisfies

$$E[\sup_{0 \leq t \leq T} ||u(\cdot, t)||^2] \leq C[1 + E[||h||^2]] \tag{C.4}$$

For some constant $C > 0$ depending on T.

Proof. See Chow[2007], p.g 72-74

The proof is mainly concerned with first truncating the system 2.39 such that $f_n(u, v, x, t) = f(J_n u, v, x, t)$ and the same for σ where $J_n u = \zeta_n(||u||)u$ then the conditions $C_n.1, C_n.2$ imply that f_n, σ_n satisfy the global conditions $C1, C2$. Then to proof conditon $C3$ we use inequalities which are derived from the first stage of the proof. Then to prove $C4$ we use the energy inequality to show the existence of the global solution. From this we are able to show

$$u(\cdot, t) = \lim_{n \implies \infty} u^n(\cdot, t)$$

Hence a global solution is claimed for u. The same can also be repeated for v. ∎

Bibliography

[1] Pérez-Rodríguez, L., Jovani, R. and Stevens, M., 2017. Shape matters: animal colour patterns as signals of individual quality. Proceedings of the Royal Society B: Biological Sciences, 284(1849), p.20162446.

[2] Murray, J., 1981. A Pre-pattern formation mechanism for animal coat markings. Journal of Theoretical Biology, 88(1), pp.161-199.

[3] Andersson, L., 2020. Mutations in Domestic Animals Disrupting or Creating Pigmentation Patterns. Frontiers in Ecology and Evolution, 8.

[4] Wang, M., Tsanas, A., Blin, G. and Robertson, D., 2020. Predicting pattern formation in embryonic stem cells using a minimalist, agent-based probabilistic model. Scientific Reports, 10(1).

[5] Landge, A., Jordan, B., Diego, X. and Müller, P., 2020. Pattern formation mechanisms of self-organizing reaction-diffusion systems. Developmental Biology, 460(1), pp.2-11.

[6] Krupinski, P., Chickarmane, V. and Peterson, C., 2011. Simulating the Mammalian Blastocyst - Molecular and Mechanical Interactions Pattern the Embryo. PLoS Computational Biology, 7(5), p.e1001128.

[7] Schneider, I. and Ellenberg, J., 2019. Mysteries in embryonic development: How can errors arise so frequently at the beginning of mammalian life?. PLOS Biology, 17(3), p.e3000173.

[8] Yang, S., Fan, Z. and Ren, R., 2021. The Stochastic Resonance Phenomenon of Different Noises in Underdamped Bistable System. Advances in Mathematical Physics, 2021, pp.1-9.

[9] Peszat, S. and Zabczyk, J., 2007. Stochastic partial differential equations with Levy noise. Cambridge: Cambridge University Press.

[10] KIM, J. and KISH, L., 2006. RECOGNIZING DIFFERENT TYPES OF STOCHASTIC PROCESSES. Fluctuation and Noise Letters, 06(01), pp.L1-L6.

[11] Sun, G., Jin, Z., Li, L. and Liu, Q., 2009. The role of noise in a predator–prey model with Allee effect. Journal of Biological Physics, 35(2), pp.185-196.

[12] Scarsoglio, S., Laio, F., D'Odorico, P. and Ridolfi, L., 2011. Spatial pattern formation induced by Gaussian white noise. Mathematical Biosciences, 229(2), pp.174-184.

[13] Hori, Y. and Hara, S., 2012. Noise-induced spatial pattern formation in stochastic reaction-diffusion systems. 2012 IEEE 51st IEEE Conference on Decision and Control (CDC),.

[14] GADGIL, C., LEE, C. and OTHMER, H., 2005. A stochastic analysis of first-order reaction networks. Bulletin of Mathematical Biology, 67(5), pp.901-946.

[15] Székely, T. and Burrage, K., 2014. Stochastic simulation in systems biology. Computational and Structural Biotechnology Journal, 12(20-21), pp.14-25.

[16] Karig, D., Martini, K., Lu, T., DeLateur, N., Goldenfeld, N. and Weiss, R., 2018. Stochastic Turing patterns in a synthetic bacterial population. Proceedings of the National Academy of Sciences, 115(26), pp.6572-6577.

[17] Turing, A., Philosophical Transactions of the Royal Society of London. Series B, Biological Sciences, 1952. The chemical basis of morphogenesis. 237(641), pp.37-72.

[18] FitzHugh R. (1969) Mathematical models of excitation and propagation in nerve. Chapter 1 (pp. 1-85 in H.P. Schwan, ed. Biological Engineering, McGraw-Hill Book Co., N.Y.)

[19] Nagumo J., Arimoto S., and Yoshizawa S. (1962) An active pulse transmission line simulating nerve axon. Proc IRE. 50:2061–2070.

[20] G. Nicolis and I. Prigogine, 1977, Self-Organization in Nonequilibrium Systems, Wiley-Interscience.

[21] Schnakenberg, J., 1979. Simple chemical reaction systems with limit cycle behaviour. Journal of Theoretical Biology, 81(3), pp.389-400.

[22] Etheridge, A., Freeman, N., Penington, S. and Straulino, D., 2017. Branching Brownian motion and selection in the spatial Λ-Fleming–Viot process. The Annals of Applied Probability, 27(5).

[23] Fontes, L., Isopi, M., Newman, C. and Ravishankar, K., 2002. The Brownian Web. Proceedings of the National Academy of Sciences, 99(25), pp.15888-15893.

[24] Murray, J. D. (2002), Mathematical Biology I. An Introduction , Vol. 17 , Springer , New York

[25] Jiang, W., Takeshita, N., Maeda, T., Sogi, C., Oyanagi, T., Kimura, S., Yoshida, M., Sasaki, K., Ito, A. and Takano-Yamamoto, T., 2021. Connective tissue growth factor promotes chemotaxis of preosteoblasts through integrin 5 and Ras during tensile force-induced intramembranous osteogenesis. Scientific Reports, 11(1).

[26] Maini, P., 2004. Using mathematical models to help understand biological pattern formation. Comptes Rendus Biologies, 327(3), pp.225-234.

[27] MAREE, A., 2002. Modelling Dictyostelium discoideum Morphogenesis: the Culmination. Bulletin of Mathematical Biology, 64(2), pp.327-353.

[28] Flowers, J., Li, S., Stathos, A., Saxer, G., Ostrowski, E., Queller, D., Strassmann, J. and Purugganan, M., 2010. Variation, Sex, and Social Cooperation: Molecular Population Genetics of the Social Amoeba Dictyostelium discoideum. PLoS Genetics, 6(7), p.e1001013.e

[29] Zheng, Q., Wang, Z., Shen, J. and Iqbal, H., 2017. Turing Bifurcation and Pattern Formation of Stochastic Reaction-Diffusion System. Advances in Mathematical Physics, 2017, pp.1-9.

[30] Lord, G., Powell, C. and Shardlow, T., 2013. An introduction to computational stochastic PDEs. 1st ed.

[31] Kloeden, P. and Platen, E., 1999. Numerical solution of stochastic differential equations. 1st ed. Berlin: Springer.

[32] Hausenblas, E., Randrianasolo, T. and Thalhammer, M., 2020. Theoretical study and numerical simulation of pattern formation in the deterministic and stochastic Gray–Scott equations. Journal of Computational and Applied Mathematics, 364, p.112335.

[33] Kelkel, J. and Surulescu, C., 2009. On a stochastic reaction–diffusion system modeling pattern formation on seashells. Journal of Mathematical Biology, 60(6), pp.765-796.

[34] Hopf E (1942) Abzweigung einer periodischen Lösung von einer stationären Lösung eines Differentialsystems. Ber Verh Sachs Akad Wiss Leipzig Math-Nat 94:3–22

[35] MARSDEN, J., McCRACKEN, M., CHERNOFF, P., CHILDS, G. and CHOW, S., 1976. The Hops bifurcation and its applications. New York: Springer.

[36] Hollis, S., Martin, Jr., R. and Pierre, M., 1987. Global Existence and Boundedness in Reaction-Diffusion Systems. SIAM Journal on Mathematical Analysis, 18(3), pp.744-761.

[37] Henry, D., 1981. Geometric theory of semilinear parabolic equations. Berlin: Springer-Verlag.

[38] Chow, P., 2015. Stochastic Partial Differential Equations, Second Edition. Hoboken: CRC Press.